ARDB Technical Note 134-Draft 11/10/97 **E158**

Overview of Cavity Beam Position Monitors for Precision Møller Scattering Measurements

David H. Whittum, Roger A. Erickson, Yury G. Kolomensky, Mike B. Woods, and Gerald Yocky

After a short, motivational review of SLAC-Proposal-E-158, and the requirements on the beam, we discuss the matter of resonant cavities as employed for phase and position sensitive pickups, for an S-Band bunched beam, concentrating, on the "linac-style" cavity system. We then analyze the intrinsic features of the signal delivered by the cavity. We go on to sketch the front-end electronics required for BPM signal acquisition and processing. We conclude with a summary of the very large amount of work remaining to prepare for the E158 experiment.

This is the first note in a series on the E158 BPM system. Other notes as yet are:
ARDB TN 152: Mode Classification in Non-Axisymmetric Structures: How Nonlinear Can a Cavity Be?
ARDB TN 153: Beam Excitation of a Non-Axisymmetric Structure: Higher-Moments, Common Mode, Output-Coupling, Resonant and Non-Resonant Operation
ARDB TN 154: Introduction to the Phase-Cavity for the Linac Resonant Cavity Beam Position Monitor System

Outline

1. Introduction

In this introduction we review the Proposal E-158,[1] providing a condensed synopsis of the motivation and gross beam requirements. It shoud be understood that this synopsis relates the work of the entire E-158 collaboration. We go on to examine in more detail requirements on beam phase-space. After brief mention of other beam parameters, we choose to concentrate on beam position measurements as they would be employed to discern beam centroid, pointing angle, and energy on a pulse-to-pulse basis. We review the particulars of cavity beam position monitors (BPM's) as they have been employed historically at SLAC. We then consider the particular requirements of the E158 experiment, the status of E158-related BPM studies, and summarize the known questions remaining. Throughout we make note of the work, including experimental studies with beam, remaining to be performed to certify the required performance of BPM's for E-158.

1.1 Synopsis of Proposal E-158

It has been proposed to employ Møller scattering of a polarized electron beam on the atomic electrons of an unpolarized liquid hydrogen target, in End Station A, to measure the left-right asymmetry, A_{LR}, at low center-of-mass frame squared transverse momentum, $Q^2 \approx 10^{-2}\ \mathrm{GeV}^2$. The motivation for this is that the cross-section for the interaction depicted in Fig. 1 may be calculated very precisely in the Standard Model, and thus a precision measurement of this cross-section may be employed to accurately discern deviations from the Standard Model. With the set-up depicted in Fig.2, the left-right asymmetry will be inferred from the difference over many pulses between calorimeter readouts for a left-circularly polarized beam and a right-circularly polarized beam. New physics one might find includes:

(1) a new neutral gauge boson (Z')
(2) a new contact interaction, corresponding to electron compositeness on a length scale Λ_{ee}. The reach of this experiment would extend to $\Lambda_{ee} \approx 11\ \mathrm{TeV} \equiv 1/2 \times 10^{-18}\ \mathrm{cm}$, and, could, for example, uncover an interaction mediated by a doubly charged Higgs boson Δ^{++}
(3) oblique corrections to the cross-section, due to virtual particles with masses in the TeV range.

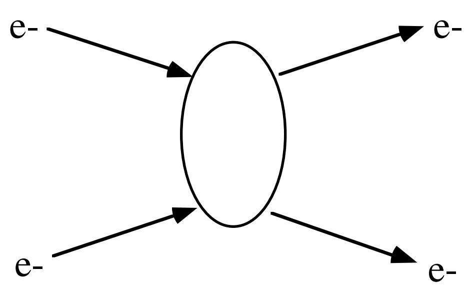

FIGURE 1.1. The cross section for Moller scattering will include interaction mediated by the photon, the *Z*, and, corrections at the 30% level due to higher-order diagrams involving loops with quarks, *W*, γ and *Z*.

The setup is depicted in cartoon fashion in Fig. 2, and consists of an electron beam produced in the Two-Mile Linac complex,[2] impinging on a liquid hydrogen target 1.5 m in length,

[1] "A Precision Measurement of the Weak Mixing Angle in Møller Scattering", R. Carr, *et al.*, K.S. Kumar, coordinator, SLAC-Proposal-E-158, Version Dated July 17, 1997.
[2] *The Two-Mile Accelerator*, R. B. Neal, ed., (W. A. Benjamin, New York, 1968) pp. 500-516. We will refer to this reference as the "Blue Book".

and 3 inches in diameter. A somewhat more ambitious cartoon can be seen in Fig. 3. With each pulse, a 5 kJ "blowtorch" of ejecta and disrupted beam will emerge from the target, and pass through a chicane, and four quadrupoles. The magnets will bring scattered electrons with momenta from 12-24 GeV/c to the calorimeter, situated 60 m from the target entrance, stretching in the radial direction, from 17 cm to 26 cm from the beamline axis, and covering 360° in azimuth in eight octants. Most of the 500 kW average power will pass through the center hole of the annulus formed by the detector, and will dissipate itself harmlessly in a beam dump.

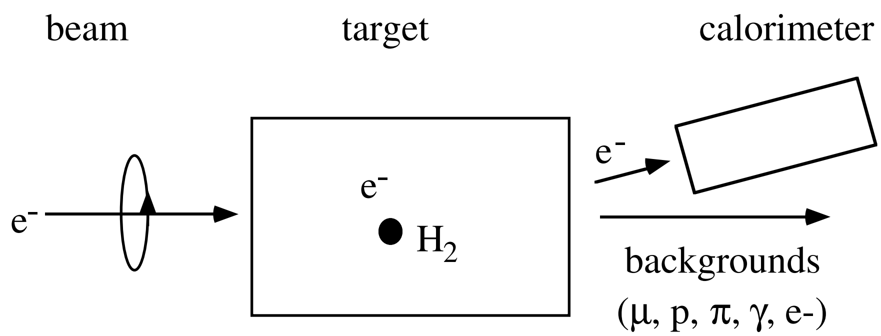

FIGURE 1.2. The cross section for Moller scattering will be inferred from experiments with a fixed target of liquid hydrogen, and a polarized beam from the Two-Mile accelerator. The primary detector will be a calorimeter constructured from a sandwich of 3 mm tungsten plates acting as Cerenkov radiators, and quartz fibers to guide the radiation to detectors. Use of a Cerenkov radiator insures only a small response to background particles such as: muons, pions, photons, hadrons, heavy ions and assorted nuclear ejecta.

Requirements on the beam and the beamline instrumentation for this experiment can be understood from the following considerations. The left-right asymmetry is by definitition, the asymmetry in cross-sections σ_R and σ_L, for right and left-handed electrons, $A_{LR} = (\sigma_R - \sigma_L)/(\sigma_R + \sigma_L)$. It is proposed to infer A_{LR} from inferred values for differential cross-sections integrated over the calorimeter solid angle. Theses cross-sections are to be inferred from (1) calorimeter flux integrated over each machine pulse, and summed over all machine pulses and (2) a normalization flux inferred from readout of a luminosity monitor. The luminosity monitor will consist of quartz fibers wrapped around the beam-pipe downstream of the target, and is intended to monitor elastic electron-proton scattering.

The theory of electroweak interactions, predicts at tree-level (in the Born approximation) that A_{LR} computed from the differential cross-sections at center of mass polar angle Θ is

$$A_{LR} = \left(\frac{m_e c^2 E\, G_F}{2^{1/2} \pi \alpha} \right) \frac{16 \sin^2 \Theta}{\left(3 + \cos^2 \Theta\right)} g_{ee},$$

where the fine-structure constant, the Fermi coupling constant, and the electron mass are[3]

$$\alpha \approx 1/137.0359895(61),\ \ G_F/(\hbar c)^3 \approx 1.16639(2) \times 10^{-5}\,\mathrm{GeV}^{-2},\ \ m_e c^2 \approx 0.51099906(15)\,\mathrm{MeV}.$$

The quantity g_{ee} may be related to the Weinberg or weak-mixing angle,

$$g_{ee} = \frac{1}{4} - \sin^2 \theta_W,$$

[3] "Review of Particle Physics", Particle Data Group, *Phys. Rev. D*, **54** (1996) 65.

and its value at this mass-scale (this range of Q^2) is quite uncertain, thought to lie in the range $g_{ee} \approx 1-2\times10^{-2}$. This result for A_{LR}, with a 40% reduction due to higher order processes gives $A_{LR} \approx 2\times10^{-7}$, corresponding to what one would measure with 100% beam polarization. The specific goal of the experiment is simply to infer $\sin^2\theta_W\left(Q^2\right)$ at the level $\delta\sin^2\theta_W \approx 8\times10^{-4}$, with 80% beam polarization This requires $\delta g_{ee}/g_{ee} \approx 6\times10^{-2}$, and thus $\delta A_{LR} \approx 1\times10^{-8}$. One can go on to infer that statistical errors are a major factor in this experiment.

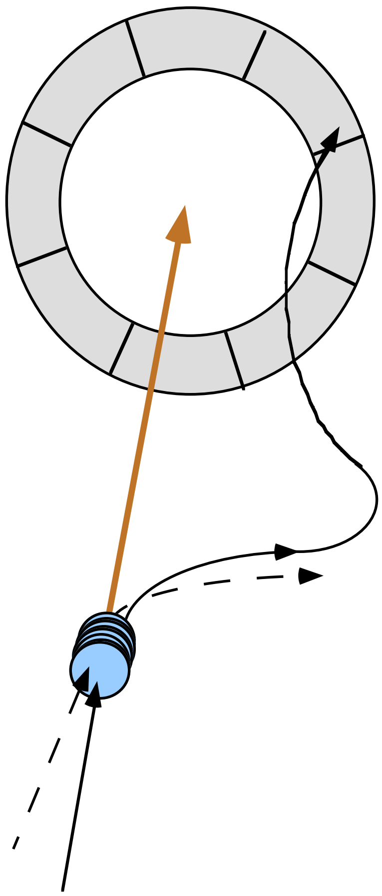

FIGURE 1.3. Illustration of the beam hitting the target, producing Moller electrons that strike the segmented calorimeter. Notice that if the beam enters at an angle or an offset, flux collected by the calorimeter may be influenced.

If one imagines numerous trials in each of which N events are recorded, one expects statistical fluctuations in the results with an rms $1/N^{1/2}$. Since δA_{LR} will be computed roughly by "counting" one should expect to make use of a sample at least as large as $N \approx 1/\left(\delta A_{LR}\right)^2 \approx 1\times10^{16}$. This has implications for the beam intensity and beam time required.

The number of electrons scattered into the detector may be expressed as $N = TL\sigma_M$, where T is the time for which both the accelerator, the detector and all sub-systems are "up" and operating together, σ_M is the Møller differential cross-section integrated over the solid angle covered by the detector to be employed, and L is the luminosity. Theoretical luminosity is a product of two factors, one from the accelerator, and one from the target; it is given by $L = \left(N_b f_{rep}\right)\left(n_t l\right)$, where

N_b is the number of beam electrons per pulse, $f_{rep} = 120$ Hz is the pulse repetition frequency, n_t is the number density of scatterers in the target (assumed larger than the beam and uniform in the region of the beam.) The target length $l \approx 150\,\mathrm{cm}$. The mass density of liquid hydrogen is 0.07 gm/cm^3, corresponding to a number density of $n_t \approx 4\times10^{22}$ cm^{-3} and $n_t l \approx 6\times10^{24}$ cm^{-2}. As a point of reference, for $N_b \approx 1\times10^{11}$, this corresponds to $L \approx 8\times10^{37}\,\mathrm{cm}^{-2}\mathrm{s}^{-1}$. A run-time of 5 months was thought to be economically resonable given the prospective benefits of the experiment to our understanding of high-energy physics. This corresponds to $T \approx 1\times10^7\,\mathrm{s}$, with no allowance for down-time, and an integrated luminosity of $LT \approx 8\times10^{44}\mathrm{cm}^{-2} \approx 8\times10^{14}\,\mu\mathrm{barn}^{-1}$, where $1\ \mathrm{barn} = 10^{-24}\mathrm{cm}^2$. The spectrometer was designed to accomodate center-of-mass scattering angles Θ over the range $-0.5 < \cos\Theta < 0$ ($120° > \Theta > 90°$), and this acceptance corresponds to scattered electron energies in the range $E' \approx 10 - 25$ GeV. The Moller differential cross-section (in the Born approximation), integrated over this angular acceptance gives a cross-section $\sigma_M \approx 14\,\mu\mathrm{barn}$ for a 50 GeV beam. This determines the total number of Møller-scattered electrons to be detected $N = TL\sigma_M \approx 10^{16}$.

However, a more precise statistical analysis together with an assumed 50% "up-time" (reducing T by $\times 2$) raises the required number of events, and puts the required charge per pulse at $N_b \approx 4-6\times10^{11}$, for 48.3 GeV and 45 GeV respectively.[4] Total number of machine pulses will be $N_p = f_{rep}T \approx 1.2\times10^9$, and the total number of beam electrons will be $N_p N_b \approx 5-7\times10^{20}$.

As a check of these considerations, Monte Carlo simulations were performed using the code GEANT, and indicated that for 10^7 incident electrons, 690 Møller-scattered electrons enter the detector, a fraction 7×10^{-5}. On this basis, one would expect $7\times10^{-5}\times\left(5-7\times10^{20}\right) \approx 4-5\times10^{16}$ scattered electrons to be collected, in agreement with the foregoing estimates.

1.2 Effect of Møller Beam Parameter Fluctuations on A_{LR}

With these considerations in mind let us turn to consider the effect of beam parameters on the systematics of the experiment. The problem is illustrated schematically in Fig.4, a one-dimensional version of Fig. 3.

According to GEANT the "beam" of Møller-scattered electrons impinging on the detector (from 16.75 cm to 26 cm in radius) is characterized by an energy distribution varying from 0.2 at 10 GeV to 1.0 at 14 GeV to 0.0 at 28 GeV. The rms spot size at the detector corresponds to $\sigma_x \approx \sigma_y \approx 5.6\,\mathrm{mm}$ and the distribution appears to be somewhere between a Gaussian and a Bennett distribution.[5] In one pulse the number, N_M, of scattered electrons intercepted by the detector may be expressed as an integral over the detector aperture,

$$N_M = \iint_D d^2\vec{r}_{\perp D}\, F\left(\vec{r}_{\perp D}\right),$$

of the single-pulse time-integrated flux of these electrons $F\left(\vec{r}_{\perp D}\right)$. Generally speaking, there will be upstream fluctuations (unrelated to the weak interaction) producing a fluctuation δN_M on each machine pulse. Let us see how big these can be, and then work backward to assess the requirement on the beam.

---

[4] A thorough analysis of the linac remains to be performed to confirm the feasibility of these numbers (chosen based on scaling of the cross-section with energy, and the need for a convenient spin-rotation measurement).

[5] See Fig. 9, p. 25 of the proposal.

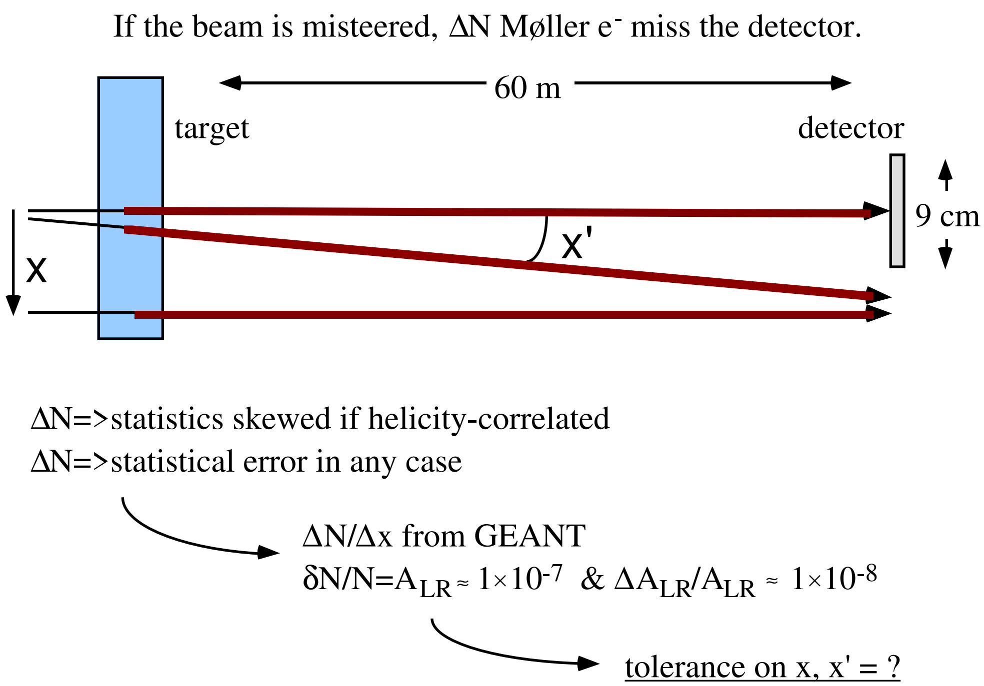

FIGURE 1.4. Illustration of the systematics problem associated with beam position and angle for E-158.

Let us summarize the results of one experiment (one 5-month run) in terms of a collection of numbers N_{mL}, N_{mR}. We assume $2M$ machine pulses with $m=1,2,...,M$ pulses with left-handed polarization, and the same number of pulses with right-handed polarization. (That is to say the total number of pulses is $2M = N_p \approx 1.2\times 10^9$.) For that experiment we may compute

$$a_{LR} = \sum_L N_{mL} - \sum_R N_{mR}.$$

Let us suppose that the numbers N_{mL} are distributed about a mean N_L according to a Gaussian with rms σ_N, and similarly for N_{mR}. That is to say, $N_{mL} = N_L + \sigma_N r_{Lm}$, and $N_{mR} = N_R + \sigma_N r_{Rm}$, where the stochastic variables r_{Lm}, r_{Rm} follow a Gaussian distribution with unit rms, and are, we suppose uncorrelated. After many such experiments, we could examine averages over these experiments and arrive at a mean value,

$$\langle a_{LR}\rangle = \left\langle \sum_L N_{mL} \right\rangle - \left\langle \sum_R N_{mR} \right\rangle.$$

Our confidence in this value would depend on the scatter, which we could assess by consulting the variation in a_{LR} over this sample of experiments, $\Delta a_{LR} = a_{LR} - \langle a_{LR}\rangle$. Over the course of many trials, each of $2M$ machine pulses, and absent any systematic errors, we would find

$$\left\langle (\Delta a_{LR})^2 \right\rangle = \sigma_N^2 \left\langle \left(\sum_L r_{Lm} - \sum_R r_{Rm} \right)^2 \right\rangle \approx \sigma_N^2 2M,$$

and we would thus find an rms in our a_{LR} measurement of $\sigma_{aLR} \approx \sigma_N \sqrt{2M}$. Meanwhile, the quantity of interest is

$$A_{LR} = \frac{\sum_L N_{mL} - \sum_R N_{mR}}{\sum_L N_{mL} + \sum_R N_{mR}} \approx \frac{a_{LR}}{2M\overline{N}},$$

where in the last line we make use of the fact that $\overline{N} = \left(N_L + N_R\right)/2 \approx N_L \approx N_R$. Evidently the rms in our measurement will be

$$\sigma_{ALR} \approx \frac{\sigma_{aLR}}{2M\overline{N}} \approx \frac{\sigma_N}{\overline{N}} \frac{1}{\sqrt{2M}}.$$

We require this number to be of order 10% of A_{LR} itself, so that $\sigma_{ALR} \le 10^{-8}$. Expecting that a fraction 7×10^{-5} of incident beam electrons result in Møller scattered electrons in the detector, we can put $\overline{N} \approx 7\times10^{-5}\times4\times10^{11} \approx 3\times10^{7}$, and thus require

$$\sigma_N \le \overline{N}\sigma_{ALR}\sqrt{2M} \approx 3\times10^7\times10^{-8}\times\sqrt{1.2\times10^9} \approx 1\times10^4 \qquad \Leftrightarrow \qquad \sigma_N/\overline{N} \approx 3\times10^{-4}.$$

So, for results from this experiment to be interesting, one must be able to bound or identify and tag any non-electroweak effects (in the injector, linac, BSY, A-Line, target, drift, detector) that could result in random fluctuations in the combined probability of Moller electron production and transmission to the detector at the level $\sigma_N/\overline{N} \approx 3\times10^{-4}$. To emphasize, we are quite free to lose large numbers of Møller electrons, provided we do so in a consistent fashion, without spurious helicity-correlation.

To appreciate this number, $\sigma_N \approx 1\times10^4$, note that it corresponds to a charge of 1fC or 0.2 pA of average current. Using the conversion factor of 7×10^{-5}, it corresponds to 1.4×10^8 beam electrons (23 pC), or 3 nA on average. For illustration, for 2×10^{11} beam electrons per pulse (32 nC) and a 300 ns pulse train (107 mA), the number of beam electrons per bucket (per S-Band wavelength) is 2×10^8. We should emphasize that the σ_N constraint does not imply that beam electron pulse fluctuations must be held to 10^8 ($\delta N_b/N_b \approx 3\times10^{-4}$). We are quite free to lose beam electrons in an erratic fashion, provided that they are not "lost" in such a way that they still show up on the luminosity monitor. The more hard to discern consequences are for the state of the beam itself, absent beam loss: what changes in the beam could lead to a fluctuation of 10^4 Møller electrons?

To answer this let us start with the Møller electron distribution on the target and work backwards. The picture is that of Fig. 5. The analysis depends heavily on the shape of the tails of the Møller distribution and can only be accurately examined through Monte Carlo simulations, such as with GEANT. Nevertheless let us try to make some analytic progress. We suppose the distribution is cylindrically symmetric about its axis, albeit perhaps displaced from the detector axis. We express the number density per unit area (time-integrated flux per unit area) at the plane of the detector as

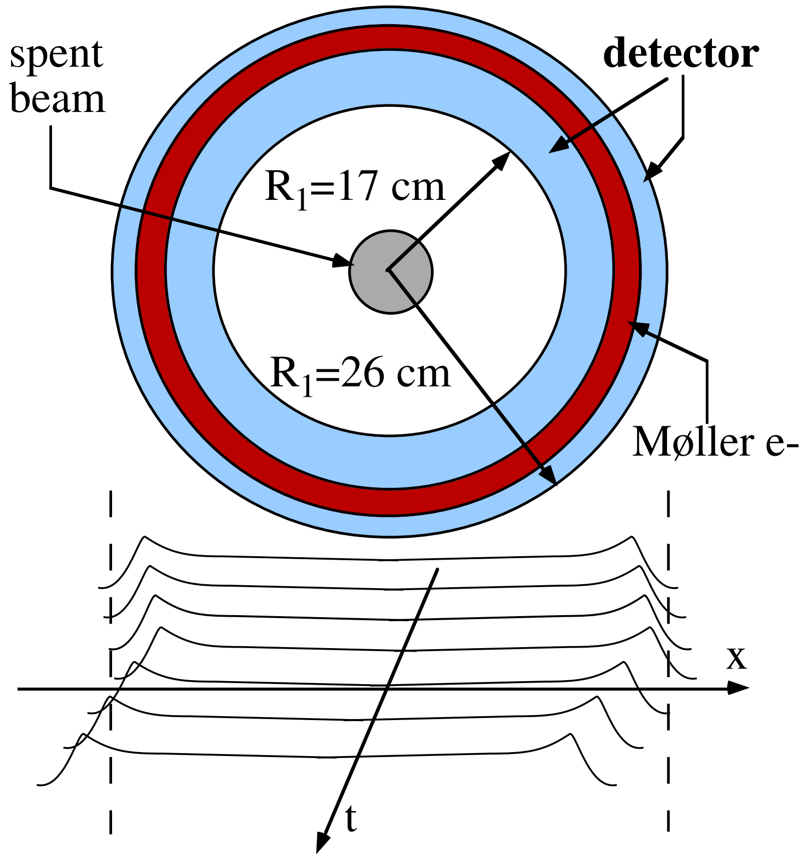

FIGURE 1.5. Motion of the Møller "beam" on a pulse-to-pulse basis would modify the flux recorded by the calorimeter. How sensitive the calorimeter reading is to this motion depends on the shape of the tails of the Møller distribution.

$$F(\vec{r}_{\perp D}) = f(|\vec{r}_{\perp D} - \vec{r}_{\perp B}|).$$

and we consider a horizontal offset $\vec{r}_{\perp B} = x_B \hat{x}$. We expand in the small offset, adopting detector-centered polar coordinates, $r = \sqrt{x^2 + y^2}$, $x = r\cos\phi$, $y = r\sin\phi$,

$$F(r,\phi;x_B) = f\left(\sqrt{(x - x_B)^2 + y^2}\right) = F(r,\phi;0) + x_B \frac{\partial F}{\partial x_B}(r,\phi;0) + \frac{1}{2} x_B^2 \frac{\partial^2 F}{\partial x_B^2}(r,\phi;0) + \ldots ,$$

where

$$\frac{\partial F}{\partial x_B}(r,\phi;x_B) = f'\left(\sqrt{(x - x_B)^2 + y^2}\right)\frac{(x - x_B)}{\sqrt{(x - x_B)^2 + y^2}}, \qquad \frac{\partial F}{\partial x_B}(r,\phi;0) = f'(r)\frac{x}{r},$$

$$\frac{\partial^2 F}{\partial x_B^2}(r,\theta;0) = f''(r)\frac{x^2}{r^2} - f'(r)\frac{y^2}{r^3}.$$

Thus the Taylor expansion is

$$F(r,\theta;x_B) = f(r) + x_B f'(r)\frac{x}{r} + \frac{1}{2}x_B^2\left(f''(r)\frac{x^2}{r^2} - f'(r)\frac{y^2}{r^3}\right) + \ldots \; .$$

We assume our detector is annular with inner radius R_1, outer radius R_2, and a hard edge. Then

$$N_M(x_B) = \iint\limits_D d^2\vec{r}_{\perp D}\, F(\vec{r}_{\perp D}) = \int\limits_0^{2\pi} d\phi \int\limits_{R_1}^{R_2} r\,dr = 2\pi\int\limits_{R_1}^{R_2} r\,dr f(r) + \frac{\pi}{2}x_B^2\int\limits_{R_1}^{R_2} r\,dr\left(f''(r) - f'(r)\frac{1}{r}\right) + \ldots$$
$$= N_M(0) + \delta N_M,$$

where, after an integration by parts,

$$\delta N_M = \frac{\pi}{2}x_B^2\{rf'(r) - 2f(r)\}\Big|_{r=R_1}^{r=R_2}.$$

In this way, if one knows the density at the detector edge, and the slope, one can compute the sensitivity to beam offsets, which is evidently always quadratic. Let us consider a simple two-parameter distribution,

$$f(r) \approx \frac{2N}{\pi\, r_0\, a}\left\{1 + \frac{(r-r_0)^2}{a^2}\right\}^{-2},$$

and the normalization assumes $r_0 >> a$. We find

$$\delta N_M = -2N\frac{x_B^2}{r_0\, a}\left\{\frac{\left[(r^2 - r_0^2)/a^2 - 1\right]}{\left[(r-r_0)^2/a^2 + 1\right]^3}\right\}\Bigg|_{r=R_1}^{r=R_2}.$$

For an initially centered distribution $r_0 = (R_1 + R_2)/2$, we have

$$\frac{\delta N_M}{N_M} = -4\frac{x_B^2}{a^2}\frac{(R_2 - R_1)/a}{\left[1 + (R_2 - R_1)^2/4a^2\right]^3}.$$

For the planned-for Moller detector, dimensions are $R_2 - R_1 \approx 9.25\,\mathrm{cm}$, and for illustration we take $a = 0.5\,\mathrm{cm}$. Then,

$$\frac{\delta N_M}{N_M} \approx -1.1\times 10^{-4}\,\frac{x_B^2}{a^2}.$$

For Gaussian-distributed offsets x_B, with mean zero, and rms σ_{xB}, we obtain an offset in the mean count, and an rms fluctuation in count,

$$\frac{\overline{\delta N_M}}{N_M} \approx -1.1\times 10^{-4}\,\frac{\sigma_{xB}^2}{a^2}, \qquad \frac{\sigma_N}{\overline{N}} \equiv \left\{\overline{\left(\frac{\delta N_M}{N_M}\right)^2} - \left(\frac{\overline{\delta N_M}}{N_M}\right)^2\right\}^{1/2} \approx -1.1\times 10^{-4}\,\frac{\sigma_{xB}^2}{a^2},$$

and we make the approximation of small fluctuations. Imposing our requirement $\sigma_N/\overline{N} \approx 3\times 10^{-4}$

, we find $\sigma_{xB} \approx 1.6a \approx 0.8\,\mathrm{cm}$. This strikes one as quite a loose tolerance on position on the detector.

Further inspection of Fig. 9 (p. 25) in the proposal suggests that a better fit would move the distribution off the center of the aperture, putting the peak in the distribution at r=24 cm. Adjusting the scale a numerically to insure an *rf(r)*-weighted rms about the mean of 0.5 cm, we find $a \approx 0.58\,\mathrm{cm}$, the distribution appears as depiced in Fig. 1.6 (with scale chosen to ease comparison with Fig. 9 of the proposal). Our flux sensitivity coefficient is then larger by a factor of 60,

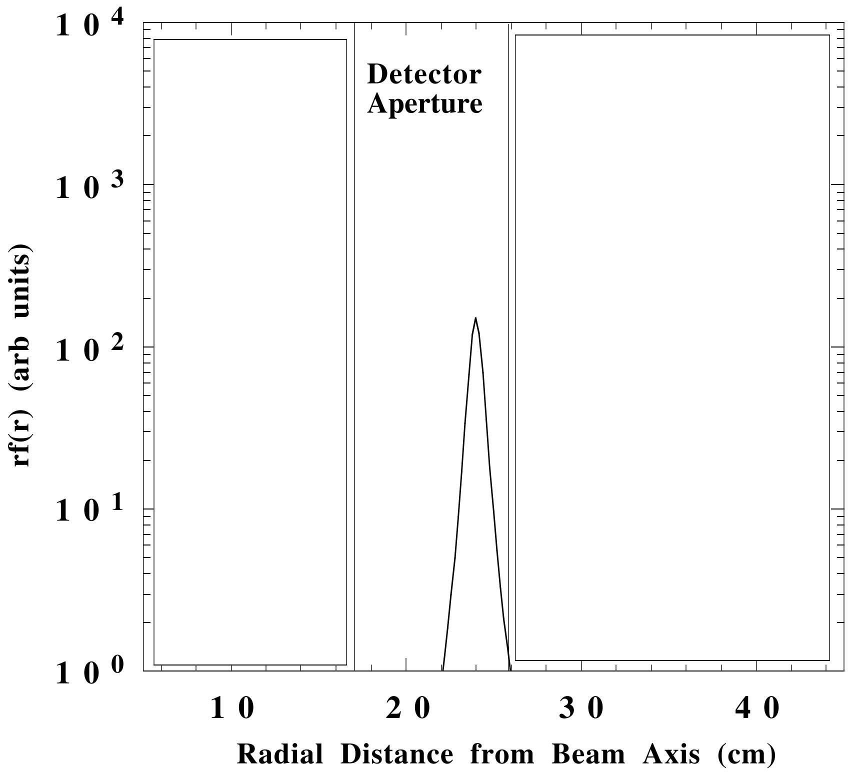

FIGURE 1.6. Model distribution for Møller flux, attempting to fit the GEANT output of Fig. 9 (p.25) of the proposal, with a two-parameter distribution.

$$\frac{\delta N_M}{N_M} = -6.5 \times 10^{-3}\,\frac{x_B^2}{a^2}. \qquad \text{(best eyeball fit to Fig. 9)}$$

Our tolerance on Moller scattered beam position is then $\sigma_{xB} \approx 0.2a \approx 0.1\,\mathrm{cm}$.

Next let us work our way back to the target. If we were to consider transport from the target as a drift of length $L \approx 60\,\mathrm{m}$, the tolerance, $\sigma_{xB} \approx 0.2a \approx 0.1\mathrm{cm}$ would translate into a position tolerance of this amount at the target, and an angle tolerance of $\sigma'_{xL} = \sigma_{xB} / L \approx 16\,\mu rad$.

We could be concerned though that this view of the transport as drift however is too simple. Transport from the 1.5 m target is governed by a chicane, four quads, and a drift, as indicated in Fig. 1.7.[6] The quadrupoles collect Moller electrons scattered into 4.5-7.2 mrad and put them on the detector. Note that Moller electrons appear throughout a 1.5 m length, corresponding to the channel transited by the incident beam of rms width $\sigma_x \approx \sigma_y \approx 1$ mm.

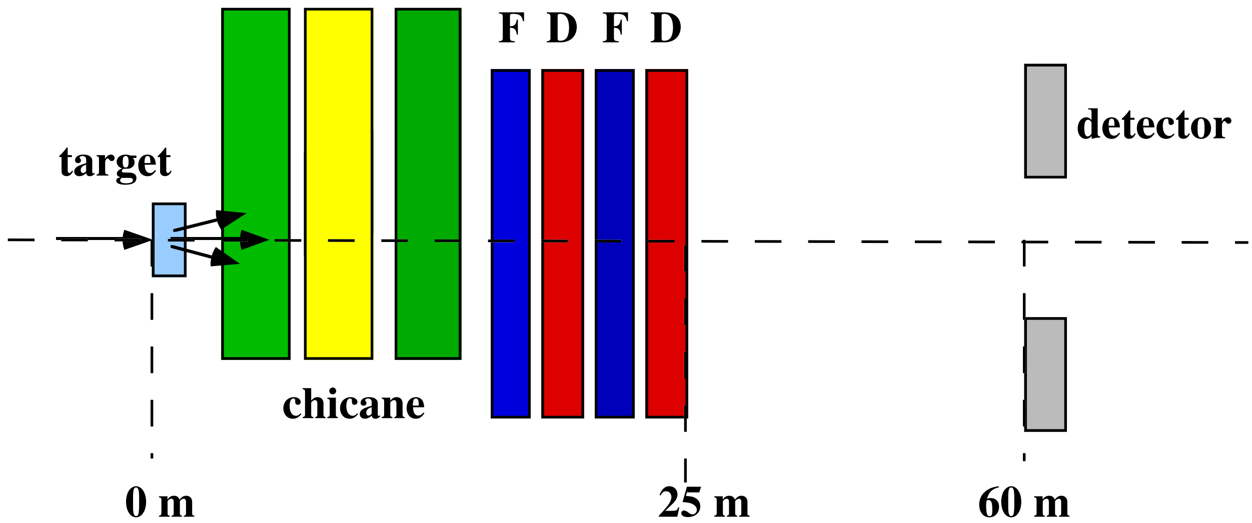

FIGURE 1.7. Optics for the Møller electrons are determined from one chicane, four quads and a drift length of 35 m. [check origin of coordinates, question of target left side, target center, see Fig. 8, p. 24 proposal].

At first-order (neglecting coupling and chromatic effects) we may characterize the optical system in terms of a matrix $\mathbf{R}$.[7] In this approximation (crude for a wide momentum-distribution with collimation) transport of the x-phase-space from the target to the detector is governed by

$$\begin{pmatrix} x \\ x' \end{pmatrix}_D = \mathbf{R}\begin{pmatrix} x \\ x' \end{pmatrix}_T = \begin{pmatrix} R_{11} & R_{12} \\ R_{21} & R_{22} \end{pmatrix}\begin{pmatrix} x \\ x' \end{pmatrix}_T .$$

To determine our tolerance on motion at the target, we must use the elements R_{11}, R_{12} for the system depicted in Fig.1.7. (And similarly for y, where the corresponding elements are referred to as R_{33}, R_{34}, the subscripts making reference to a 6-dimensional matrix for the 6-dimensional phase-space). The $\mathbf{R}$-matrix may be computed from an input deck describing the magnets and their locations, and such a calculation appears to have been performed for the proposal, with and without quads, as is evident from Fig. 8 of the proposal.

Making use of the $\mathbf{R}$-matrix one may relate quantities at the target to those at the detector,

---

[6] The outer bends in the chicane are the 12D125 dipoles (B202 and B204 from the 20 GeV/c spectrometer) and the inner bend is a 22D136 (B81, from the 8 GeV/c spectrometer). The four quads are 15Q31 elements (Q82 and Q83 from the 8 GeV/c spectrometer and Q82, Q83 from the 20 GeV/c spectrometer). The function of the chicane (an achromat) is to obscure the detector from backgrounds with help from collimators.

[7] There are many good references on this subject: Karl L. Brown, "First and Second Order Matrix Theory for the Design of Beam Transport Systems and Charged Particle Spectrometers", SLAC-Report-75 (June, 1982); K. Brown and R. Servranckx, "First and Second Order Charged Particle Optics", SLAC-PUB-3381 (July 1984); *The Optics of Charged Particle Beams*, David C. Carey (Harwood, Chur, 1987); K. L. Brown, *et al.*, “Transport” (Users Manual), SLAC-91, Revised.

$$\langle x_D \rangle = R_{11}\langle x_T \rangle + R_{12}\langle x'_T \rangle, \qquad \sigma_{xD}^2 = R_{11}^2\sigma_{xT}^2 + 2R_{11}R_{12}\sigma_{xx'T} + R_{12}^2\sigma'^2_{xT}.$$

Here we denote

$$\sigma_{xD}^2 = \langle x_D^2 \rangle - \langle x_D \rangle^2, \quad \sigma'^2_{xD} = \langle x'^2_D \rangle - \langle x'_D \rangle^2, \quad \sigma_{xx'D} = \langle x_D x'_D \rangle - \langle x_D \rangle \langle x'_D \rangle,$$

where $\langle \mathrm{K} \rangle$ indicates an average over the beam (a single shot quantity, not an rms over many pulses). At the target, position and angle are uncorrelated so that

$$\sigma_{xD}^2 = R_{11}^2\sigma_{xT}^2 + R_{12}^2\sigma'^2_{xT}.$$

We can infer the $\mathbf{R}$-matrix elements we need by inspection of Fig. 8 of the proposal (p.24).[8] One can see that at the target, the Møller population has spot size $\sigma_y \approx 0.4$ mm and $\sigma_x \approx 1.6$ mm. At the detector, without quads, one sees $\sigma_y \approx 7.1$ mm and $\sigma_x \approx 8.0$ mm at the detector. With the quads, $\sigma_x \approx \sigma_y \approx 5.4$ mm.With quads off, we have a drift, and the $\mathbf{R}$-matrix is given by

$$\mathbf{R} = \begin{pmatrix} 1 & L \\ 0 & 1 \end{pmatrix},$$

and the spot-size at the detector is

$$\sigma_{xD}^2 = \sigma_{xT}^2 + L^2\sigma'^2_{xT}.$$

With quads on the beam spot is not greatly reduced, and one may expect, based on Fig. 8, that $R_{12} \approx 0.8\,L$. It seems reasonable to take $R_{11} \approx 1$, and in light of this, to accept our estimates of position tolerances based on the simplest picture of the spectrometer as a drift. We conclude that the tolerance on the Møller scattered beam launch position and angle on the target is

$$\sigma_{xT} \approx 1000\ \mu\text{m}\ , \qquad\qquad \sigma'_{xT} \approx 16\ \mu rad.$$

These tolerances translate directly into tolerances on the linac electron beam on-target. Clearly the position tolerance on-target is quite loose. The angular tolerance however is tight. This is because, in the linac, angle and position are related, and with a typical beta function of order $\beta \approx 20\,\text{m}$, a $16\ \mu rad$ angle corresponds to a 300 µm oscillation. To be more precise, let us consider a a picture as in Fig. 1.8. If the target is at a waist we can relate angle jitter there to position jitter at a point P, π/2 upstream in machine phase, according to $\sigma'^2_{xT}\beta_+ = \varepsilon = \sigma_{xP}^2 / \beta_+$. This implies $\sigma_{xP} = \sigma'_{xT}\sqrt{\beta_+\beta_-}$. Naturally we become interested in the actual lattice to be employed [revise later to include config]. For purposes of illustration we could note that in a FODO lattice, we have the relation $\beta_+\beta_- = 4f^2$, where f is the focal length of the quad. Focal length is determined from gradient and effective length according to

[8] Taking $\sigma'_x \approx 4.5\times10^{-3}$, and $\sigma_x \approx 1.6\times10^{-3}$ m, after 60 m of drift, would expect a 270 mm rms size at the detector. The difference must be collimation (?).

$$\frac{1}{f(\mathrm{m})} \approx 0.2998 \frac{g(\mathrm{T/m})}{E(\mathrm{GeV})} l_e(\mathrm{m}).$$

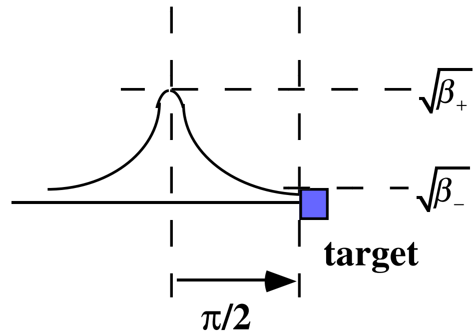

FIGURE 1.8. Measurement of beam angle at the target will require measurement of beam position. The accuracy required of the beam position measurement depends on the optics.

Gradient in term is determined by the quadrupole aperture $2R$, and the pole tip field B_p (limited to about 1 T), and is then given by $g=B_p/R$. As a point of reference, there are two standard beam switchyard quadrupoles[9] [revise for more recent info]. The "8-cm" quads have g=7.5 T/m, and l_e=2m, while the "18.6-cm" quads have g=4.33 T/m and l_e=2m. At 50 GeV these would correspond to focal lengths of 11.1 m and 19.3 m respectively. Taking the smaller bore quad and assuming 40 GeV as an example, this would imply

$$\sigma_{xP} \approx 17.8\ \mathrm{m} \times \sigma'_{xT} \approx 17.8\ \mathrm{m} \times 16\ \mu\mathrm{rad} \approx 280\ \mu\mathrm{m}.$$

Before moving on to consider linac beam motion and position measurement, let us note that the angular tolerance computed here is larger by a factor of 160 than that called for in the proposal (Table 6, p. 32). This matter should be discussed. Meanwhile, in the following sections, we will employ the premise that angular motion of the beam at the level of

$$\sigma' \approx 0.1\ \mu rad \qquad \text{(specification pending revision)}$$

should be detectable. This corresponds to $\sigma_{xP} \approx 1.7\ \mu\mathrm{m}$ for the "40 GeV , 8-cm quad, FODO" example used above. A later version of this note should incorporate analysis based on the actual lattice to be employed.

1.3 Orbit Analysis Requirements

The foregoing considerations suggest that a long visit to the lattice is in order. [This visit is not over as of this revision]. Let us consider the requirements on linac beam orbit analysis. A short review of optics is helpful.

In a linear lattice without coupling (no sextupole components, no skew quadrupole components, no vertical bends) we may describe beam motion according to

$$\frac{d}{ds}\gamma\frac{dx}{ds} + \hat{K}_x x = \frac{\delta\gamma}{\rho} + \frac{\delta F_x}{mc^2}, \quad \frac{d}{ds}\gamma\frac{dy}{ds} + \hat{K}_y y = \frac{\delta F_y}{mc^2},$$

where the magnetic lattice determines the functions,

[9] Blue Book, p. 620.

$$\hat{K}_x = \frac{-e}{mc}\frac{\partial B_y}{\partial x}, \qquad \hat{K}_x + \hat{K}_y = \frac{\gamma}{\rho} = \frac{1}{\gamma}\left(\frac{eB_y(r_0)}{mc}\right)^2.$$

In the absence of acceleration (*i.e.*, after the linac) and perturbations $\delta F_x, \delta F_y$, the motion in x is described by an inhomogeneous second-order equation

$$\frac{d^2x}{ds^2} + Kx = \frac{\delta}{\rho},$$

with a similar result for y (without the bend term). Here $\delta = \delta\gamma / \gamma$ is the fractional deviation in energy of the particle being considered from the "design" particle. (More precisely δ is the momentum deviation). The focusing strength defined in this way depends on particle energy (a "chromatic" effect),

$$K = \frac{-e}{mc\gamma}\frac{\partial B_y}{\partial x}.$$

For thin magnets (where the impulse recieved by a particle may be computed as an integral along the unperturbed, ballistic orbit), one has

$$\Delta x' = x\frac{e}{p}\int_{-\infty}^{+\infty} ds \ \frac{\partial B_x}{\partial y}\left(s, \vec{r}_\perp = 0\right).$$

In passing we note that the value $\int ds(\partial B_x / \partial y)$ for a given quad, for a particular linac setup ("configuration") can be found in the database in units of kG. Together with this information, one can find the quad location, and, at that location, the computed values for the various optical functions discussed below. Generically, this dataset or configuration is referred to as the "*K*-mod" or model for *K*. The actual *K*-model witnessed by the beam may differ due to: quad offset (always present at some level), quad rotation, shorted coil, reversed wiring, hysteresis, error in magnet polynomial (polynomial relating current requested from the power supply to magnet field), failure of a power supply to regulate, external interaction with a μ-boundary (adjacent magnet, support). It is straightforward to model optics for a given setup (it is much more involved to determine the optimal setup). Online software is available for orbit-fitting based on standard BPM readings. The subject of orbit fitting and on-line orbit analysis is a large one, and very popular just now at SLAC.[10]

Continuing with our optics review, there are two independent solutions to the homogeneous equation with initial conditions at a point s_0 on the beamline. One is a *"cosine-like"* solution $C(s,s_0)$ such that,

$$C(s = s_0, s_0) = 1, \qquad \frac{\partial C}{\partial s}(s = s_0, s_0) = 0.$$

---

[10] See, for example, M. Lee, *et al.*, "Lattice commissioning strategy for the B-Factory", *Proceedings of the 1997 Particle Accelerator Conference* (IEEE, New York, to be published) --- and other papers in these proceedings. SLAC experts on this subject include James Safranek, Yunhai Cai, Martin Lee and Jeff Corbett, among many notable others.

and the other is a *"sine-like"* solution $S(s,s_0)$ such that,

$$S(s=s_0,s_0)=0. \qquad \frac{\partial S}{\partial s}(s=s_0,s_0)=1.$$

A general solution may be expressed as

$$x(s)=x_0 C_\delta(s,s_0)+x_0' S_\delta(s,s_0)+D_\delta(s,s_0)\delta,$$

where the dispersion D is determined from

$$\frac{d^2 D}{ds^2}+KD=\frac{1}{\rho}.$$

Dispersion may be computed from

$$D(s,s_0)=\int_{s_0}^{s} ds' G(s,s')\frac{1}{\rho},$$

where

$$G(s,s')=H(s-s')\{S(s,0)C(s',0)-C(s,0)S(s',0)\}.$$

Absent energy errors, transport is governed by

$$\mathbf{R}(s,s_0)=\begin{pmatrix} C(s,s_0) & S(s,s_0) \\ \frac{\partial C}{\partial s}(s,s_0) & \frac{\partial S}{\partial s}(s,s_0) \end{pmatrix}.$$

An alternate expression for these functions makes use of the machine functions

$$C(s,0)=\sqrt{\frac{\beta(s)}{\beta(0)}}(\cos\psi+\alpha(0)\sin\psi), \qquad S(s,0)=\sqrt{\beta(s)\beta(0)}\sin\psi,$$

$$\mathbf{R}(s,0)=\begin{pmatrix} \sqrt{\frac{\beta(s)}{\beta(0)}}(\cos\psi+\alpha_0\sin\psi) & \sqrt{\beta(s)\beta(0)}\sin\psi \\ \frac{(\alpha_0-\alpha)\cos\psi-(1+\alpha_0\alpha)\sin\psi}{\sqrt{\beta(s)\beta(0)}} & \sqrt{\frac{\beta(0)}{\beta(s)}}(\cos\psi-\alpha\sin\psi) \end{pmatrix}.$$

The machine functions satisfy

$$\psi(s)=\int_0^s ds'\frac{1}{\beta(s')}, \qquad \frac{d^2}{ds^2}\sqrt{\beta(s)}+\hat{K}\sqrt{\beta(s)}=\frac{1}{\sqrt{\beta(s)}}, \qquad \alpha(s)=-\frac{1}{2}\frac{d\beta}{ds}.$$

Next let us turn to the problem of orbit fitting. Uncertainties in this problem are of two types: (1) BPM errors (scale, offset, *x-y* coupling, linearity, cables mislabeled, BPM’s multiplexed and misleading one in subtle ways) and (2) Model Errors (listed above). In the simplest case, with no errors, and no dispersion, one observes a betatron oscillation on a collection of beam position monitors numbered *k=1,...n*. Accepting a model for the lattice, embodied in cosine-like and sine-like functions, one chooses launch variables (x_0, x_0') as fit parameters in such a way as to minimize the rms error, Δ, in the fit,

$$\Delta^2 = \frac{1}{N}\sum_{k=1}^{N}\left\{x_{BPM}(n) - x_0 C(s_n) - x_0' S(s_n)\right\}^2 .$$

One can show that this is accomplished with the choice,

$$\begin{pmatrix} x_0 \\ x_0' \end{pmatrix} = \frac{1}{\overline{C^2}\,\overline{S^2} - \left(\overline{SC}\right)^2}\begin{pmatrix} \overline{S^2} & -\overline{SC} \\ -\overline{SC} & \overline{C^2} \end{pmatrix}\begin{pmatrix} \overline{Cx} \\ \overline{Sx} \end{pmatrix},$$

where the vertical bar represents an average over the bpm positions. With such a fit, and a trusted model, one may then infer the angle of the beam at any point in the lattice. This approach is premised on having at least two BPM's not degenerate with eachother (separated by a machine phase advance not near a multiple of π). The rms error in this fit, together with the rms errors in the BPM readings, added in quadrature, give one an estimate of the error in the measured beam position, relative to the reference orbit defined with recourse to the BPMs. To the extent that this reference orbit suffers unmonitored drifts, the rms of the drifts adds in some fashion as well. In this note we will concentrate primarily on the BPM readout and associated systematics (Sec. 2), but it is good to emphasize that there is more to the problem.

In practice, the model has errors, and in fact, orbit fitting is the most powerful tool for diagnosing such errors. For purposes of model-checking, one may employ averaging to beat down BPM errors, and one may wish to employ a 5x5 matrix, fitting for $(x_0, x_0', y_0, y_0', \delta)$. Clearly the more BPM's one has and the more averaging one does, the smaller the error bars will be on the model. This is interesting if the plan is to take the model, with its error bars, and perform single-shot orbit analysis to track beam angle on target.

We leave for a separate technical note, the problem of orbit fitting and orbit error analysis for E-158. This analysis is logically required in order to derive BPM requirements corresponding to the target angle requirement of $\sigma' \approx 0.1\,\mu rad$. Let us, in the meantime, accept the E-158 proposal requirements as written. Beam position monitoring with single-shot resolution of $1\,\mu$m, under nominal conditions corresponding to 120 Hz pulse repetition frequency, electrons per pulse in the range 1×10^{11} (we choose a low number, 16 nC, where the BPM signal is weaker), pulse length 300 ns, corresponding to 50 mA beam current (again, taking numbers that make the BPM work harder).

Systematic concerns relating to BPM pickup that should be mentioned at the outset are: beam jitter as large as $100\,\mu$m at some points, energy spread an appreciable fraction of 1% at points of 1 m dispersion,[11] nominal beam size of $100\,\mu$m at other points, pulse-to-pulse charge fluctuations in the 1% range. Thus one has some basic questions:

(1) Is it possible to achieve 1% of spotsize and divergence for jitter?
(2) Is the aperture operationally comfortable (particularly at the high dispersion point).

[11] There is one BSY-cavity monitor where the dispersion is about 1 m (BPM-12), and there is a large bore (about 6 inch aperture) strip-line BPM where the dispersion is about 5 m (BPM-17).

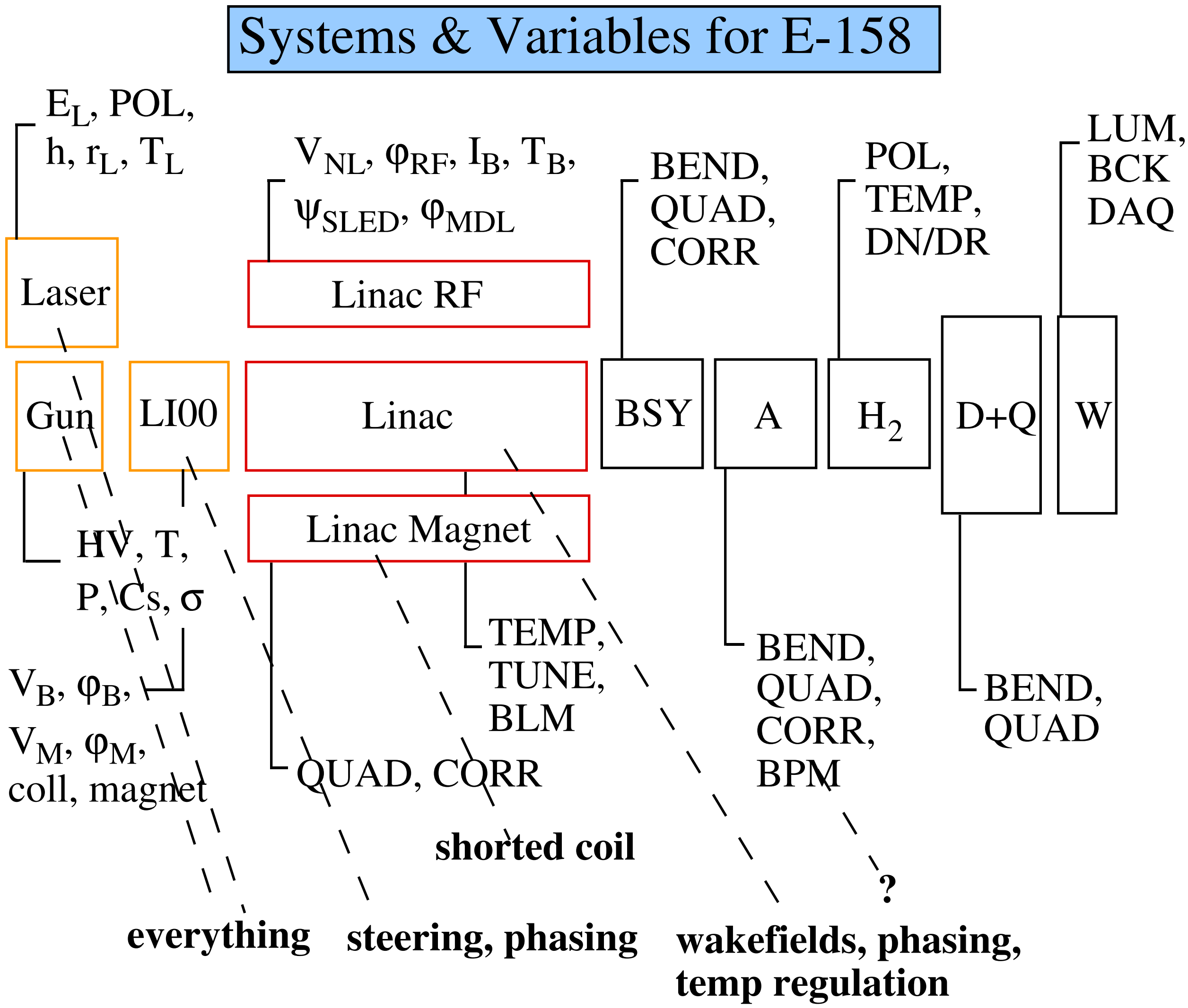

FIGURE 1.9. Major accelerator systems influencing the systematics for the E-158 experiment. Variables depicted do not form an exhaustive list.

Let us enumerate at the outset all possible contributions to the systematic errors in BPM readings. Many of these we will shortly whittle away. Figure 1.8 gives some impression of the variety of parameters and systems involved. Beam orbit conditions during the experiment will include contributions from jitter in the launched orbit amplified by wakefields in the linac, drift in the magnetic lattice, linac phasing, the selection of on-beam klystrons, and the coupling of energy jitter to transverse beam position through model and spurious dispersion at the BPM cavity locations. In addition, beam-centroid can be influenced by collimator settings even in the absence of any change to the upstream lattice and energy profile. Beam position readout is likewise influenced by numerous systematic features, including: nonlinearity in the modal fields within the position and phase cavities, form factor corrections relating to bunch length and beam-size, common-mode and higher-mode coupling in the cavities (particularly position cavities with asymmetric output coupling), cable attenuation and dispersion, dirunal drifts in cable lengths (particularly where unequal length cables and/or different cable runs are employed). Pickup on the cable from pulsed devices is an issue depending on the choice of cable. Finally, BPM reading systematics are largely influenced by the choice and particulars of the electronics. Where an external LO is employed in a mode other than free-running, phase drift between the external LO and the beam can produce systematic errors. This would be the case if a signal derived from main-drive line (MDL) or some other master-oscillator-derived and unceremoniously-transported signal is employed. Where amplifiers are employed, linearity is an issue, and where digitization is employed, bit-noise should be considered.One can be concerned too about collimation of beam tails in small apertures, and pickup from electrons that are in the process of being collimated.

In the Sec. 2, with these concerns in mind, we concentrate solely on the technical particulars of the BPM system required. Let us briefly note recent studies, as these are in part the motivation for being concerned about resolution.

2. Cavity Beam Position Monitors

2.1 Choice of Cavity

For the sake of completeness let us enumerate the cavity BPM's that have been employed on the Two-Mile Linac.[12] There are four kinds.

(1) Linac-style or In-Line Cavity Monitor --- There are many of these still installed in the linac, of which only one (BPM 30-9 in Sector 30) is connected to modern electronics and gives useful signals. These have small apertures of 0.8 in. diameter (comparable to the linac structure). [photo]

(2) BSY-style or Switchyard Monitor --- There are several of these (5 in the Common Line and A-Line) that have been used successfully. There might be two more of these in the B-Line that haven't seen a beam in years and have no electronics. The beam aperture is a 2 in. diameter. Each is a "three terminal device", with coaxial output connectors for up/down, left/right, and intensity/phase reference. [photo]

(3) 3 in. diameter aperture BPM's --- There are a few of these around, although I only know of one that works (BPM-24 in the A-Line). This is a "two-terminal device" and requires a second device (a "one-terminal" cavity) to provide the reference signal. [photo]

(4) Traveling-Wave BPM ---- There is one of these devices in End Station A just upstream of the target. It has a larger aperture than the others, and works on a different principle. There is one spare rf separator in End Station B that falls into the same category of device. [photo]

(5) Other --- In addition to these, there may be a couple devices in the radioactive scrap storage area below MCC. Two years ago one of the BSY-style BPM's was rescued from there and was cleaned up for use in the A-Line.

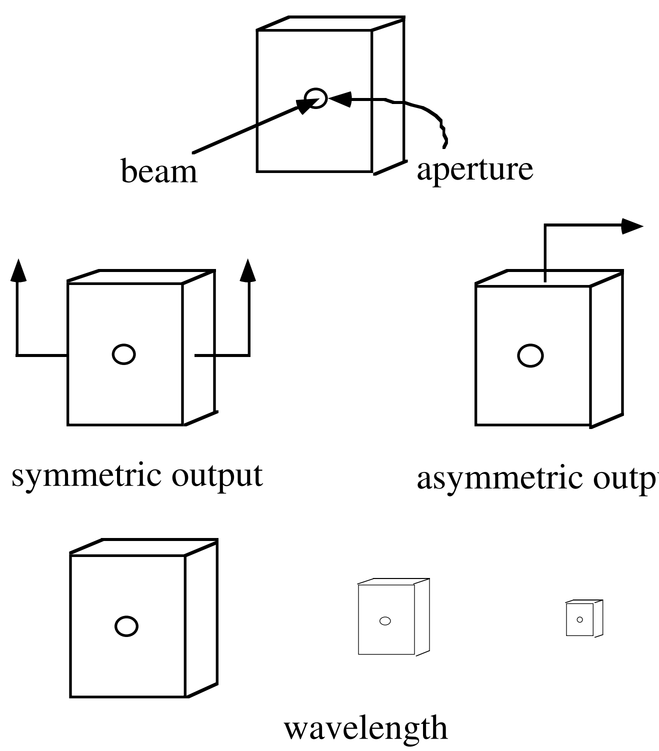

FIGURE 2.1. (a) Attributes of cavity BPM's relevant to the choice of the appropriate cavity BPM.

[12] *The Two-Mile Accelerator*, R. B. Neal, ed., (W. A. Benjamin, New York, 1968) pp. 500-516. We will refer to this reference as the "Blue Book".

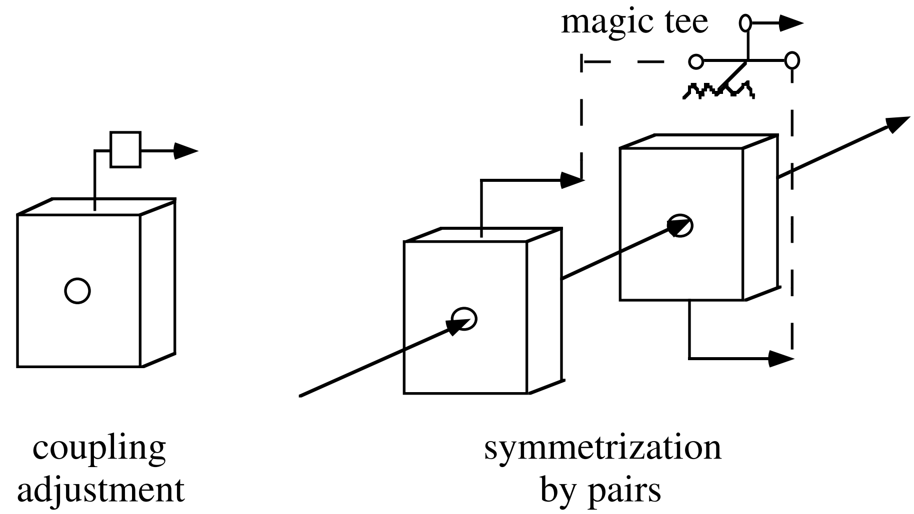

FIGURE 2.1. (b) Options for retrofitting of existing cavitiy BPM's to improve performance. Coupling adjustment with a stub tuner could be employed to raise the external *Q*. Combining of two adjacent cavity outputs in a hybrid tee could be employed for subtraction of the common mode component.

Considerations involved in the selection of the appropriate BPM include: (1) availability and/or cost of designing, fabricating and bench-testing new cavities (2) aperture for reliable current transmission in the presence of beam centroid jitter and dispersion (3) symmetric or asymmetric output (symmetrization permits subtraction of the common mode) (4) wavelength, with shorter wavelengths generally providing higher resolution, albeit at the expense of aperture, and fabrication cost. These considerations are illustrated in Fig. 2.1.

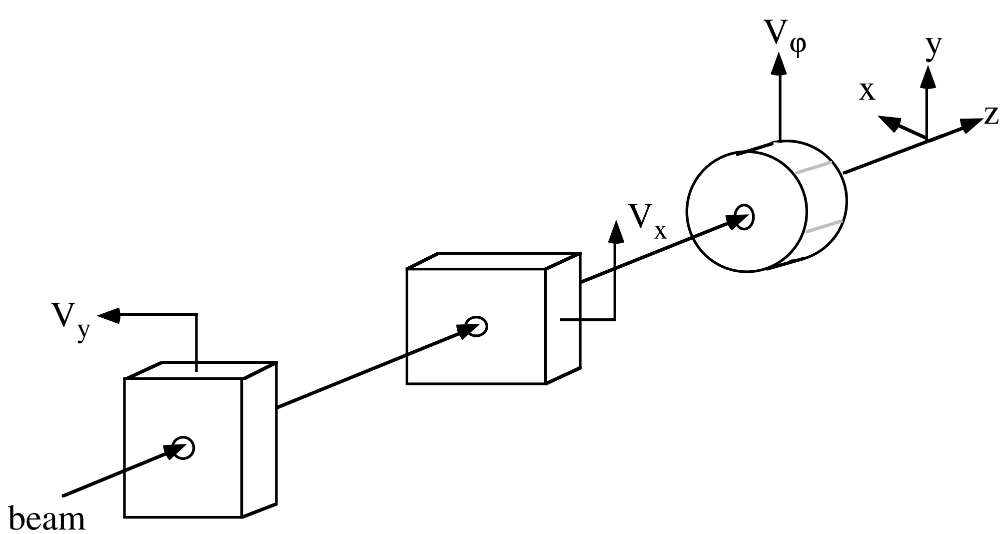

FIGURE 2.2. One BPM station includes an *x*-cavity, a *y*-cavity and a phase or φ-cavity. This sketch can be compared to Fig. 15-4 in the Blue Book (p. 504; in this figure, the girder is viewed from above)

For the work of this first note, we will consider only asymmetric output, S-Band, 0.8" diameter aperture cavities, *i.e.*, the "Linac-Style" or "In-Line" Cavity Monitors. One In-Line BPM station is illustrated schematically in Fig. 2.2. Observe that one station actually includes three cavities, an x-cavity, a y-cavity and a phase or φ-cavity. In the figure we show three symbols V_x, V_y, and V_φ.These will denote the three waveforms radiated out of the respective cavities and up the waveguide. All information we can obtain is contained in them, with the exception of calibration signals we may wish to employ, e.g., toroid reading to set the scale for V_φ;, in-situ network analysis instrumentation. Calibration signal for the x-y readouts remains unclear. In the worst (most elaborate) case, in situ movers would accomplish this. Less elaborate would be steering across the aperture of a collimator to establish orbit amplitude; steering across the aperture of the cavities with an ion-chamber as readout could be considered.

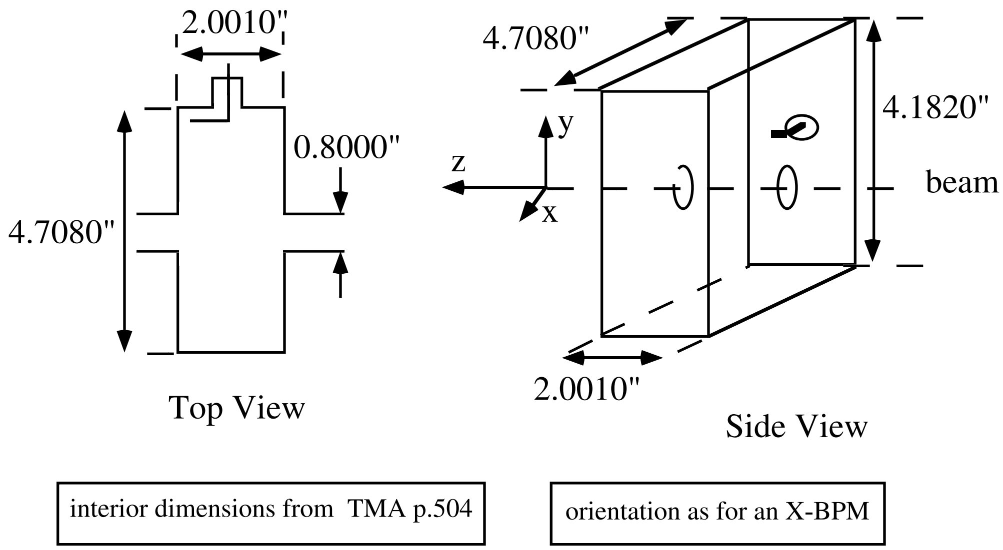

FIGURE 2.3. Major interior (electrical)dimensions for one linac-style position cavity.

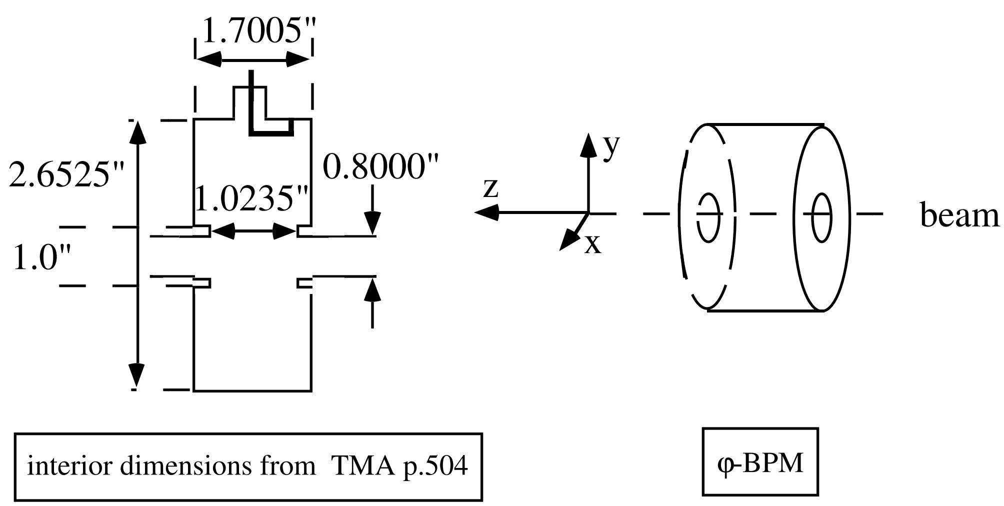

FIGURE 2.4. Major interior (electrical)dimensions for one linac-style φ-cavity.

Details of cavity dimensions are illustrated in Figs. 2.3 and 2.4. A generic beamline layout for five cavity stations for E158 is shown in Fig. 2.5. We leave for a later note the analysis (including orbit fitting analysis) that will determine the appropriate number of stations (In fact, the proposal calls for five cavities, rather than five stations; this is a minimum number.)

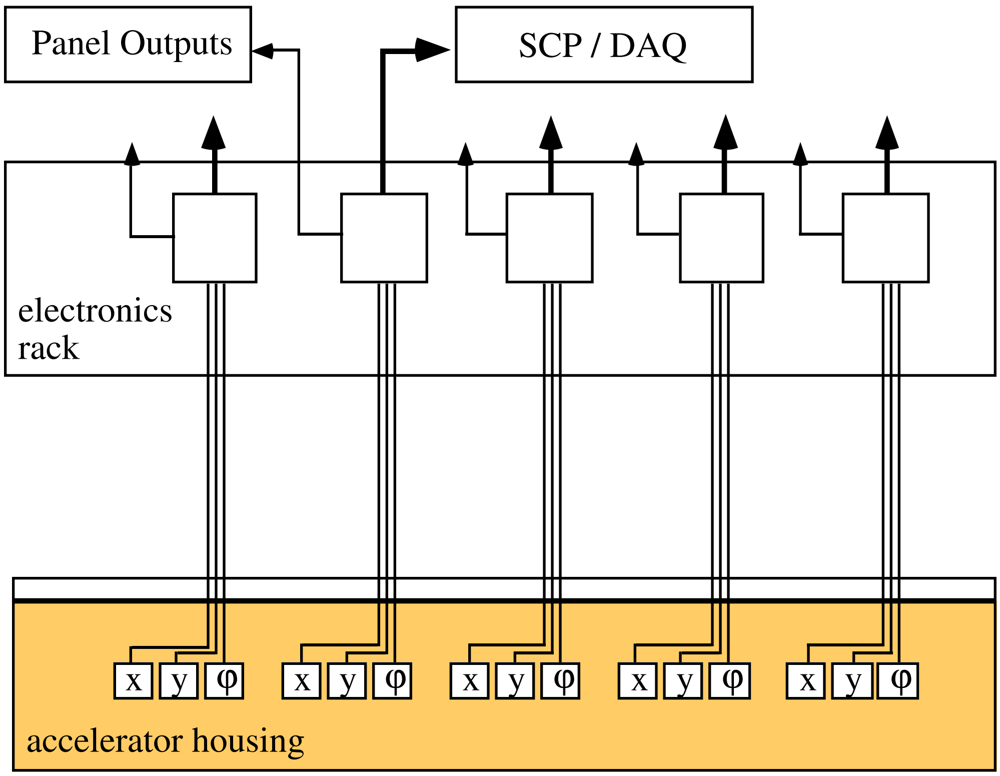

FIGURE 2.5. Generic layout of five cavity stations to indicate clearly the total number of cavities and cables. Naturally such a cartoon suggest the question: where exactly will these cavities go, and what about optics? More on this later.

Some of the issues that one contemplates in looking at Fig. 2.5 are, starting from the cavities and moving upward:

Where exactly to situate the cavities? Leave them in their present locations? What are these locations? What are the optical functions overlaid here. One station is desired at a high dispersion point; there larger aperture might be preferred, and a different cavity type indicated.

What are tolerances on cavity alignment? Cavity rotation? Cavities will need to be temperature stabilized. The Blue Book specification for these cavities is the standard 112°F as for linac sections. LCW hookups will be required, as will a temperature readout. In situ monitor of cavity tune may be desirable, provided a control variable is available for adjustment, or correction in the electronics.

What kind of cable is in place? Is it good quality (e.g., Heliax) with solid outer jacket and relatively immune to sources of pulsed noise? What is the pulsed noise environment? Do cables for one station have roughly the same length, and are they routed along a common physical path? This is of interest in accounting for diurnal phase variations due to changes in cable length.

What is the signal processing scheme? How will outputs be shared by SCP and DAQ? For commissioning, what front-panel outputs will be most useful?

What preliminary tests are required? Which cavities to use for testing? Single bunch? Multiple bunch?

How will scale factor be calibrated for the BPM's. Orbit fitting seems the most likely prospect; this requires accurate energy calibration, and accurate magnetic fields for four correctors. How accurately may correctors be calibrated? Can corrector calibration be traced to spin-rotation measurements, perhaps by test employing an opposing bend? Is an in-line, automated BPM calibration procedure required? Should triplets of cavities be employed to assess jitter?

2.2 Review of the Linac-Style Cavity System

A more detailed analysis of the linac cavities can be found in accompanying technical notes. Here we review the highlights.

2.2.1 *Review of Beams & Cavities*

A cavity mode functions as a damped harmonic oscillator, driven by the beam, and any external drive. The interest in this note is the cavity employed as a pickup, and thus we are less interested in external drive than in excitation by the beam. Coupling to the beam occurs through the beam-multipole moments, and thus it is natural to refer to a cavity mode as a monopole mode, a dipole mode and so on. In the case of a cylindrically symmetric cavity, multipoles are pure. For an asymmetric cavity more than the lowest order multipole coupling may be present.

When we speak of a beam, we will distinguish between a "bunch" and a "bunch-train" or "macropulse". A "bunch" refers to the mm (ps) length ensemble of charge residing near the crest of the S-Band (2856 MHz) accelerating waveform in the linac. For simplicity we may think of the bunch as a tri-gaussian, with current density of the form

$$J_b(x,y,\zeta) = \frac{I_b(\zeta)}{2\pi\sigma_x\sigma_y}\exp\left(-\frac{(x-x_b)^2}{2\sigma_x^2}-\frac{(y-y_b)^2}{2\sigma_y^2}\right),$$

with current waveform

$$I_b(t) = \frac{Q_b}{(2\pi)^{1/2}\sigma_t}\exp\left(-\frac{(t-t_b)^2}{2\sigma_t^2}\right).$$

Parameters are: bunch charge Q_b, bunch position (x_b, y_b), bunch size σ_x, σ_y, bunch length $c\sigma_t$ (with c the speed of light), and bunch arrival time t_b (more usually referred to in terms of bunch phase).

Excitation of a monopole mode may be qunatified in terms of the cavity V_c, coupling to forward and reverse voltages V_F, V_R in the connecting guide, and the beam current waveform I_b, according to

$$\left\{\frac{d^2}{dt^2}+\frac{\omega_0}{Q_L}\frac{d}{dt}+\omega_0^2\right\}V_c = 2\frac{\omega_0}{Q_e}\frac{dV_F}{dt}+\frac{1}{2}\omega_0\left[\frac{R}{Q}\right]\frac{dI_b}{dt}.$$

This equation comes with the picture of Fig. 2.6. The resonant angular frequency for the mode is ω_0. The strength of the coupling of between the cavity and the waveguide is quantified by $1/Q_e$, the reciprocal external Q.This adds with a term due to wall dissipation, $1/Q_w$, the reciprocal wall quality factor, to determine the loaded Q according to $1/Q_L = 1/Q_e + 1/Q_w$. The strength of coupling to the beam may be quantified by the [*R/Q*], parameter, a single geometrical entity that has no particular relation to wall losses or external coupling. Very often one prefers to refer to the loss factor for the mode, $k_l = \omega_0[R/Q]/4$. Other standard nomenclature includes: the loaded fill time $T_f = 2Q_L/\omega_0$, the unloaded shunt-impedance $R = Q_w[R/Q]$, the loaded shunt-impedance $R_L = Q_L[R/Q]$, and the coupling parameter $\beta = Q_w/Q_e$. We may also refer to some not-so-standard quantities: the damping decrement time $T_0 = 2Q_w/\omega_0$, the loaded damping rate $\nu = \omega_0/Q_L$, and the angular frequency with damping correction $\Omega = \sqrt{\omega_0^2 - \nu^2/4}$.

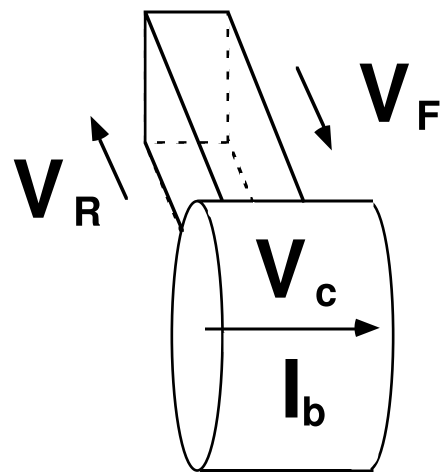

FIGURE 2.6. Sketch of the dynamic variables for a single cavity mode coupled to a waveguide fundamental mode, and a beam.

Energetics can be summarized in terms of the energy stored in the cavity,

$$U_c = \frac{\left|\tilde{V}_c\right|^2}{\omega_0[R/Q]} ,$$

expressed in terms of the phasor amplitude $\tilde{V}_c$ of the oscillating cavity voltage. Power flowing into the cavity is given by

$$P_w = \beta\frac{\left|\tilde{V}_F\right|^2 - \left|\tilde{V}_R\right|^2}{R},$$

where the reverse voltage satisfies a field-continuity condition, $V_F + V_R = V_c$.

In the case of a cavity that is not azimuthally symmetric, but respects inversion symmetry in x & y (this covers all cases of interest to us), the conventional description given above must be modified somewhat. Namely, the current drive term must be multiplied by a quantity,

$$\langle X\rangle \approx 1 + \varepsilon_{NQ}\left(x_b^2 - y_b^2 + \sigma_x^2 - \sigma_y^2\right) + \ldots ,$$

accounting for a possible quadrupolar component to the modal fields, averaged over the beam cross-section. Higher multipoles may be present as indicated by the ellipses. The parameter ε_{NQ}

quantifies the normal-quad content of the modal fields, and in general must be computed from an electromagnetic field solver (or semi-analytically, for example, by mode-matching). As indicated in other technical notes, we may neglect this effect for our work here.

In addition to the monopole mode, we are interested also in the dipole modes. The description of a dipole mode excitation in a cavity is the same, in the abstract, as the monopole mode case. The evolution of the beam-cavity-waveguide system is described by

$$\left\{\frac{d^2}{dt^2}+\frac{\omega_0}{Q_L}\frac{d}{dt}+\omega_0^2\right\}V_c'=2\frac{\omega_0}{Q_e}\frac{dV_F'}{dt}+\frac{1}{2}\omega_0\left[\frac{R_\perp}{Q}\right]\frac{d}{dt}I_b x_b,$$

expressed in terms of the on-axis voltage *gradient*, $V_c'=\partial V_c/\partial x$. We consider an x-dipole mode for definiteness. The continuity condition takes the form $V_c'=V_F'+V_R'$, stored energy is

$$U_c=\frac{\left|\tilde{V}_c'\right|^2}{\omega_0\left[R_\perp/Q\right]},$$

(the definition of $\left[R_\perp/Q\right]$). The unloaded transverse shunt impedance is $R_\perp=Q_w\left[R_\perp/Q\right]$, and it is convenient to refer to the transverse loss factor $k_\perp=\omega_0\left[R_\perp/Q\right]/4$. Net power flowing down the guide into the cavity is

$$P_w=\beta\frac{\left|\tilde{V}_F'\right|^2-\left|\tilde{V}_R'\right|^2}{R_\perp}.$$

In the case of the cavity of an asymmetric cavity, the true beam position x_b in the equation above must be replaced with a term X_b that we will refer to as the inferred beam position. In the case of a cavity with x & y inversion symmetry, this is at lowest order

$$X_b\approx x_b\left\{1+\varepsilon_{NS}\left(x_b^2-3y_b^2+3\sigma_x^2-3\sigma_y^2\right)+\ldots\right\},$$

where the coefficient ε_{NS} quantifies the normal sextupole content in the cavity-mode synchronous integral.

For this work we will be interested in at least two cavities, the linac φ-cavity, and the linac x-cavity. We provide a summary of each, based on the work described in other tech. notes.

2.2.2. T*he* φ-*Cavity*

The linac φ-cavity is depicted in Fig. 2.4, it is a cylindrical copper pillbox, perturbed by beam tubes (ID 0.8”), with nose-cones (OD 1.0”), and a loop-coupler to coaxial line. The desired operating mode is a monopole mode, the perturbed version of the TM01 mode of the pillbox. Estimates based on the unperturbed pillbox scalings give: $Q_w\approx 1.73\times 10^4$, $k_l=\omega_\lambda\left[R/Q\right]/4\approx 1.11$ V/pC, $\left[R/Q\right]\approx 220\ \Omega$, and $R=Q_w\left[R/Q\right]\approx 3.77\ \mathrm{M}\Omega$.

Actual cavity dimensions were arrived at using tabulated scalings from bench measurements, and with additional “cut & try” on the bench.[13] Final dimensions were chosen to provide a frequency 2 MHz too low prior to brazing, with the idea that frequency could be adjusted by “dimpling”. Dimensions account for corrections for the beam-port and nose-cones (to improve [*R/Q*]) and correspond to a gap of 1.02”, a cavity width of 1.7” and a cavity diameter of 2.65”. Unloaded *Q* is 9600, and loaded *Q* is 1200, corresponding to an external *Q* of 1371. The coupling parameter $\beta = Q_w / Q_e \approx 7.0$. Altenmueller and Brunet quote[14] [*R/Q*] without transit angle correction is $[R/Q]/T^2 \approx 370\ \Omega$, $T \approx 0.819$, and $[R/Q] \approx 248\ \Omega$. Shunt impedance (unloaded) is then $R \approx 2.38$ MΩ. Frequency is 2856 MHz±300 kHz, with temperature detuning of 25 kHz/°F (Blue Book) or, equivalently, 1° of tuning angle for 0.5°F (Altenmueller and Brunet). Field decrement time due to copper losses is $T_0 = 2Q_w / \omega_0 \approx 1.07\ \mu\mathrm{s}$, and the loaded fill time is $T_f = 2Q_L / \omega \approx 133\ \mathrm{ns}$.

As a check of these results, we have modelled the geometry shown in Fig. 2.4 with the code `GdfidL`.[15]

[complete, in revision]

Basic scalings for the φ-cavity are as follows. In single-bunch mode, energy deposted is given by

$$U \approx 1.11\ \mu\mathrm{J}\ Q_b^2(\mathrm{nC}),$$

and peak power radiated from the cavity is

$$P \approx 1.75 \frac{U_C}{T_f} \approx 1.75 \frac{1.11\ \mu\mathrm{J}\ Q_b^2(\mathrm{nC})}{133\ \mathrm{ns}} \approx 14.6\ W\ Q_b^2(\mathrm{nC}),$$

rising as a step-function after bunch passage, and decaying with an e-folding time of $T_f / 2 \approx 66.5\ \mathrm{ns}$. In units of decibels relative to 1 mW, dBm, this is

$$10 \log_{10} P_w(\mathrm{mW}) \approx 41.6\ \mathrm{dBm} + 20 \log_{10} Q_b(\mathrm{nC})\ .$$

For an SLD high-charge bunch of 5 nC (3.1×10^{10} electrons) this provides 56 dBm. For a single bunch of 17.5 pC (1.1×10^8 electrons) this provides 6.5 dBm. (As a point of reference, a train of such bunches arriving at 2856MHz corresponds to 50 mA). These are large signals, and noise of almost any sort (thermal, environmental, etc.) is negligible.

For a bunch-train (the intendedmode of operation) and perfect tuning to resonance with the beam, the scalings given above can be employed provided it is recognized that the effective charge is not that due to a single bunch, Q_b, but that corresponding to the amount of charge that passes through the cavity in one loaded fill-time,

---

[13] O. Altenmueller and P. Brunet, “Some RF Characteristics of the Beam Phase Reference Cavity” SLAC TN-64-51, Sept. 1964 (available from the SLAC Library).

[14] Taking acount of the fact that Altenmueller and Brunet employ a convention that [*R/Q*] is lower than ours by a factor of 2.

[15] The acronym stands for the German phrase “Gitter drüber, fertig ist die Laube” or “frame up, finished is the shack”, emphasizing the importance of the mesh generator for the finite difference algorithm.

$$Q_{beff} = I_b T_f = \frac{Q_L}{\pi} Q_b \approx 382\, Q_b.$$

Thus, with a fill time of 133 ns, 1 nC of equivalent charge corresponds to 7.52 mA of real beam current and

$$10 \log_{10} P_w(\mathrm{mW}) \approx 24.1\,\mathrm{dBm} + 20 \log_{10} I_b(\mathrm{mA}).$$

This provides a nominal 257 mW/mA^2 of sensitivity. The Blue Book quotes a value a factor of 250 mW/mA^2, as does the original technical note on the subject.[16] In passing we could note that the required sensitivity for the original application of the cavity BPM's was 200 mW/mA^2 . Nominal conditions were intended to be 300 mA corresponding to 17 kW; 50 mA would have correspond to about 500 W. These signal levels are enormous.

In the resonant mode of operation, accurate cavity tuning is required, and this requires temperature regulation. For a cavity detuning $\delta_\Omega = \Delta\Omega / \Omega << 1$, expressed in terms of the cavity tuning angle, ψ,

$$\tan \psi = 2 Q_L \delta_\Omega = 2 Q_L \frac{\Delta\Omega}{\Omega}$$

the beam-induced voltage waveform, in steady-state, is

$$V_c(t) \approx \Re \exp\left[j\Omega\left(t - t_{b0}\right)\right] I_b R_L \cos\psi e^{j\psi},$$

Altenmueller and Brunet report a tuning angle variation with temperature is 1.2° / °F (cavity detuning of 25 kHz, corresponding to $\delta_\Omega \approx 9 \times 10^{-6}$ for a 1° F cavity temperature error.) Reduction of amplitude by 0.1% corresponds to 2.6° or 2.1°F.

At first sight, one is inclined to conclude that if 1 µm resolution is desired with offsets as large as 100 µm, and if the phase-reference signal is employed for amplitude normalization, then this reference amplitude should be accurate to better than 1%. Good temperature regulation (1-2°F) would be required to accomplish this. On second thought, while good temperature regulation is indeed in order, actual errors would involve the convolution of two caviy signals, and if the cavities are similarly mistuned the effect of mistuning may cancel. We will return to this subject in a later note, under the heading of signal analysis with errors. For now we continue on to consider just the basic features that are the ingredients for such an analysis.

[16] O. Altenmueller and P. Brunet, "Some RF Characteristic of the Beam Phase Reference Cavity" SLAC TN-64-51, Sept. 1964 (available from the SLAC Library).

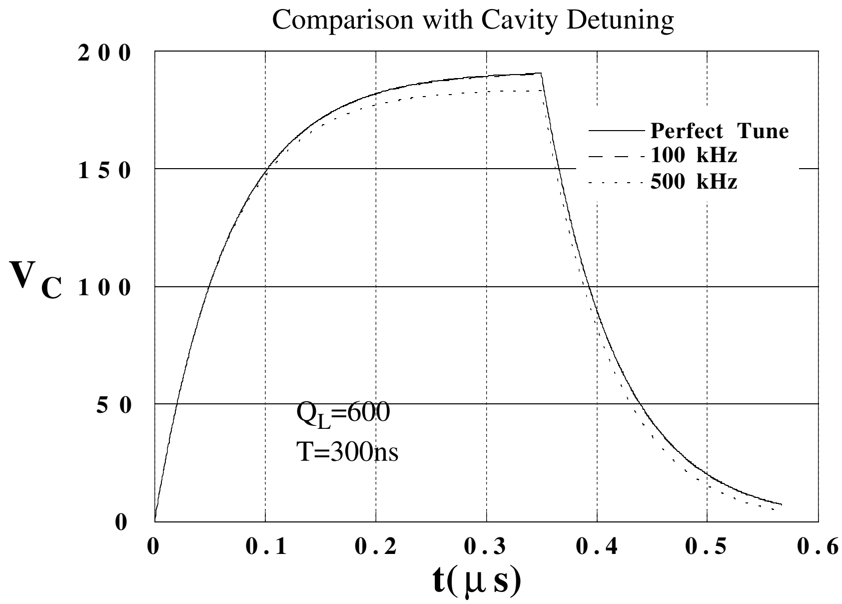

FIGURE 2.7. Result of cavity detuning in units where $2k_lQ_n$=1, for a 300 ns bunch train and a perfectly tuned cavity with Q_L=600.

For more detailed calculation of waveforms, particularly in the presence of detuning, we may express the cavity voltage as $V_c(t) \approx \Re \exp^{j\Omega(t-t_{b0})} \tilde{V}_c(t)$, referred to a "frame" rotating at the cavity angular frequency Ω, referred to the phase of the first bunch in the train, Ωt_{b0}. The phasor amplitude, after the passage of the m-th bunch is then

$$\tilde{V}_c(t_{bm}) = e^{(j\Omega-\nu/2)(t_{bm}-t_{b0})}\sum_{n=0}^{m} e^{(\nu/2-j\Omega)\tau_n}\hat{V}_{cn} = \hat{V}_{cm} + e^{(j\Omega-\nu/2)\tau_m}\tilde{V}_c(t_{bm-1}),$$

with $\hat{V}_{cn} = 2k_lQ_{bn}\exp\left(-\frac{1}{2}k_0^2\sigma_{zn}^2\right)$ the voltage amplitude contributed by bunch #n of charge Q_{bn} and bunch length σ_{zn}. The quantity $k_0 = \omega_0/c \approx 0.5986\,\mathrm{cm}^{-1}$. The bunch separation is just $\tau_n = t_{bn} - t_{bn-1} = 1/f_{RF}$, with $f_{RF} = 2856$ MHz, and assuming no phase-drift along the macropulse. This is to say that in the ideal case, of a perfectly phased beam, and a perfectly tuned cavity, $\Omega\tau_m = 2\pi$, and each bunch contribution adds in phase, with a damping decrement. The effect of detuning is illustrated with a plot of $\left|\tilde{V}_c\right|$ versus time in Fig. 2.7.

An alternate formulation employs the WKB approximation to solve the beam-cavity-waveguide equation.Expressing the beam-current waveform in terms of its first harmonic component, $I_{b0} \approx \Re\tilde{I}_{b0}e^{j\omega t}$, and expressing cavity voltage as $V_c \approx \Re\tilde{V}_ce^{j\omega t}$ we have

$$\frac{d\tilde{V}_c}{dt} + \frac{1}{T_f}\left(1 - j\tan\psi\right)\tilde{V}_c \approx k_l\tilde{I}_{b0},$$

and let us note that in general $\tan\psi = Q_L\left(\omega_0/\omega - \omega/\omega_0\right)$. This may be integrated to give

$$\tilde{V}_c(t) = k_l e^{-\Delta t}\int_0^t dt'\,\tilde{I}_{b0}(t')e^{\Delta t'},$$

with $\Delta = \left(1 - j\tan\psi\right)/T_f$, and assuming an initially unexcited cavity, and a beam current waveform arriving at t=0. Notice that a train of bunches each of charge Q_b, spaced at an interval T, and therefore of average current $I_b = Q_b/T$, corresponds to a Fourier component, or rf current, $\tilde{I}_b = 2I_b$. So, for example, for "top-hat" current waveform with droop, $\tilde{I}_{b0}(t) = 2I_b e^{-\alpha t}H(t)H\left(T_p - t\right)$, with H the step-function, one has

$$\tilde{V}_c(t) = \frac{2k_l I_b}{(\Delta - \alpha)}\begin{cases} \left(e^{-\alpha t} - e^{-\Delta t}\right) & ;\quad 0 < t < T_p \\ \left(e^{-\alpha T_p} - e^{-\Delta T_p}\right)e^{-\Delta\left(t - T_p\right)} & ;\quad T_p < t \end{cases}$$

Integrated current takes the form

$$Q_{tot}(t) = \frac{1}{2}\int_0^t \tilde{I}_{b0}(t) = I_b\begin{cases} \left(\dfrac{1 - e^{-\alpha t}}{\alpha}\right) & ;\quad 0 < t < T_p \\ \left(\dfrac{1 - e^{-\alpha T_p}}{\alpha}\right) & ;\quad T_p < t \end{cases}$$

Notice too that in general one has the relation

$$\frac{1}{2}\int_{-\infty}^{+\infty} dt\,\tilde{I}_{b0} \approx \frac{1}{2k_l}\int_{-\infty}^{+\infty} dt\left(\frac{d\tilde{V}_c}{dt} + \frac{1}{T_f}\left(1 - j\tan\psi\right)\tilde{V}_c\right) \approx \frac{\left(1 - j\tan\psi\right)}{2k_l T_f}\int_{-\infty}^{+\infty} dt\,\tilde{V}_c \approx \frac{\left(1 - j\tan\psi\right)}{R_L}\int_{-\infty}^{+\infty} dt\,\tilde{V}_c,$$

so that the cavity phasor, integrated over the full pulse provides a measure of pulse charge, subject to an overall amplitude and phase-error due to cavity mistuning.

2.2.3. *The x-Cavity*

The second cavity of interest is the "linac x-cavity", intended to function in the x-dipole mode. As indicated in Fig 2.3 this cavity consists of a rectangular pillbox, perturbed by circular 0.8" ID beam ports, without nose-cones. Lacking azimuthal symmetry, but retaining x & y inversion symmetry, one expects the first higher-order multipole to be the normal sextupole term. Estimates of cavity parameters based on the closed pillbox geometry give a mode resonant frequency of 2.8768 GHz, (20.8 MHz high), $Q_w \approx 2.26\times10^4$, $k_\perp \approx 8.07\times10^{-2}\ V/\mathrm{pC-cm}^2$, $\left[R_\perp/Q\right] \approx 17.8\ \Omega\mathrm{cm}^{-2}$ and $R_\perp \approx 4.0\times10^5\ \Omega/\mathrm{cm}^2$.

Modelling with `GdfidL` of the more realistic geometry, including the beam tubes (but excluding the coupler) gives $\left[R_\perp/Q\right] \approx 23.2\Omega\mathrm{cm}^{-2}$, $Q_w \approx 2.17\times10^4$, and permits computation of the higher order multipole content, $\varepsilon_{NS} = -4.2\times10^{-3}\mathrm{cm}^{-2}$ (and $\varepsilon_D = -4.4\times10^{-3}\mathrm{cm}^{-4}$ for the normal decapole component). This computation put the resonant frequency at 2861 MHz, and employed a numerical grid size of `STPSZE`=0.254127 cm. This work is being refined with smaller grid-size [include in revision]. The numerical geometry is depicted in Fig. 2.8, and the result for evaluation of [*R/Q*] as a function of position is illustrated in Fig. 2.9.

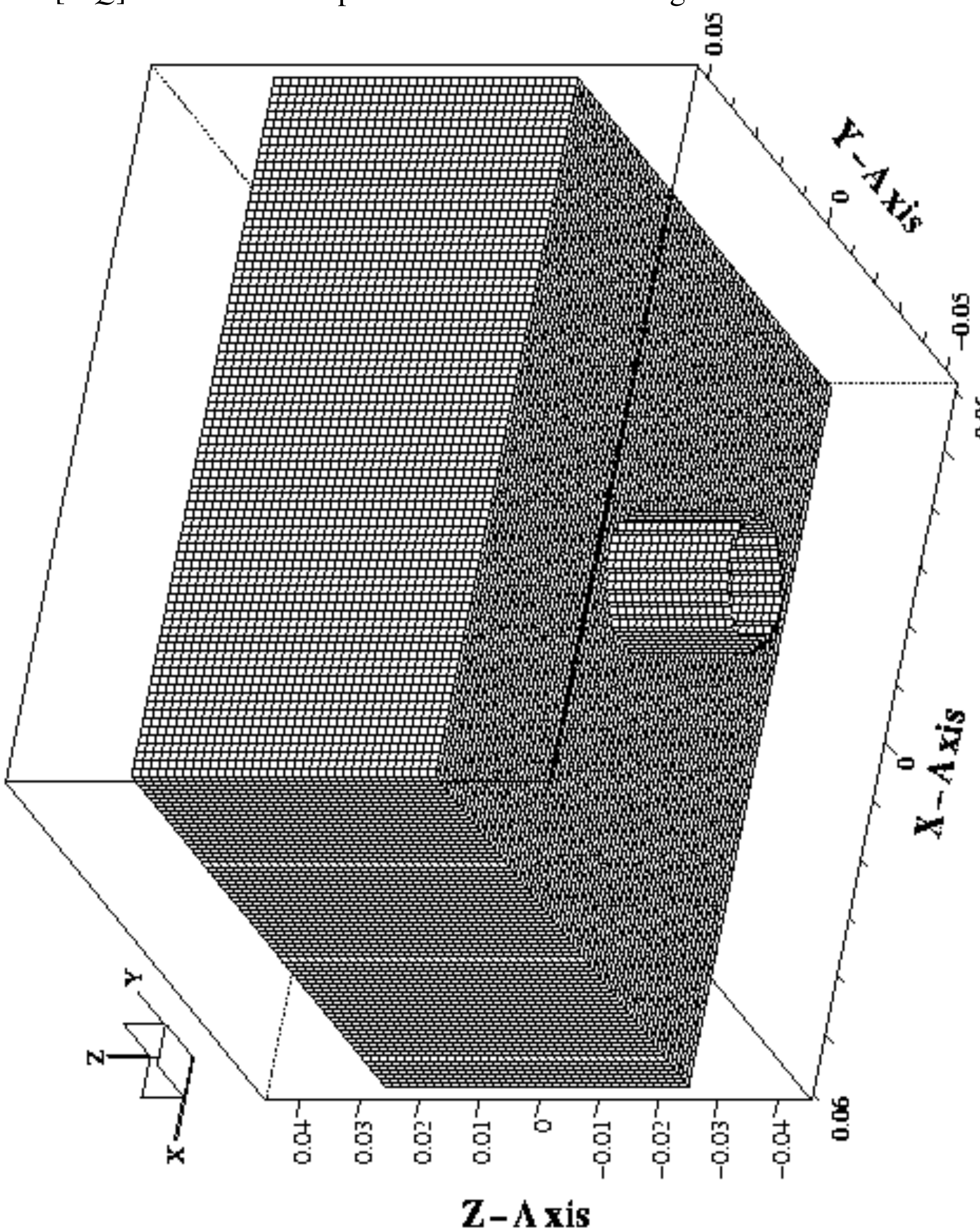

FIGURE 2.8. Geometry for the GdfidL calculation for a linac-style *x*-cavity.

The effect of field nonlinearities on induced voltage may be summarized in terms of a generalized form-factor $\exp\left(-\frac{1}{2}k_0^2\Sigma^2\right)$, replacing the usual form factor, $\exp\left(-\frac{1}{2}k_\lambda^2\sigma_z^2\right)$, where

$$\Sigma^2 \approx \sigma_z^2 - \frac{2}{k_0^2}\varepsilon_{NS}\left(x_b^2 - 3y_b^2 + 3\sigma_x^2 - 3\sigma_y^2\right),$$

The dimensionless coefficient $2\varepsilon_{NS}/k_0^2 \approx 0.023$ is computed based on the `GdfidL` results, and permits simple comparison of the effect of nonlinearities, and the usual bunch-length dependence.

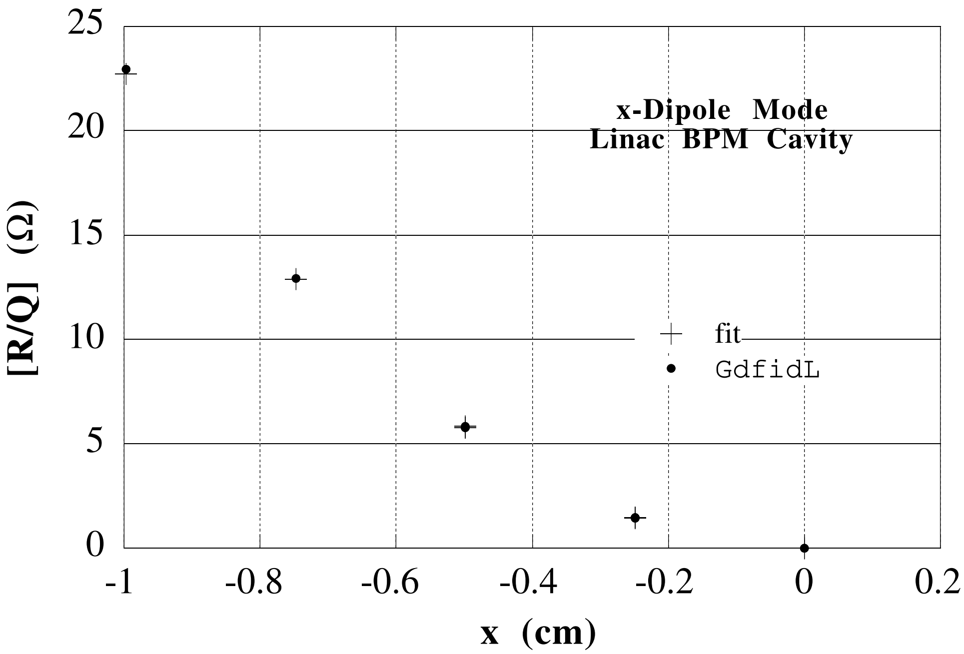

FIGURE 2.9. Comparison of the fit (including sextupole and decapole components) and the GdfidL calculation for the design mode of the linac-style *x*-cavity. The beam pipe radius is 1 cm.

The design considerations for this cavity are summarized in the report of Brunet, *et al.*.[17] They report an external Q of 300, made low to permit resolution on the 100 ns time scale. The Blue Book quotes a loaded Q of 600, unloaded Q of 15,000, and sensitivity of 100 μW/mA^{2}mm^2. The report by Brunet, *et al.*, quotes $Q_L \approx 300$ (p. 26) and lists $Q_L \approx 325$ in their Fig. 12 (p. 23), there labelled as a cold test result. (Brunet, *et al.,* explain that the motivation for the low loaded $Q_L \approx 300$ was resolution of 100 ns intervals). We will employ $Q_L \approx 325$ for loaded Q, for estimates here. Actual parameters can be measured on the bench or in situ. Accepting $Q_w = 1.5 \times 10^4$, $Q_L \approx 325$ external Q is $Q_e = 332$, and $\beta \approx 45.2$. The natural field decrement time is $T_0 = 2Q_w / \omega \approx 1.67\,\mu\mathrm{s}$, and the loaded fill-time is $T_f = 2Q_L / \omega \approx 36.2\,\mathrm{ns}$. (For the Blue Book value of $Q_L \approx 600$, $\beta \approx 24$, and $T_f \approx 67\,\mathrm{ns}$.)

For illustration let us put these numbers in practical units. We put aside the generalized form factor (Σ-term) for now. Energy deposited by a single bunch is

$$U \approx 8.07 \times 10^{-16} J \left[Q_b(\mathrm{nC}) x_b(\mu\mathrm{m})\right]^2,$$

[17] P. Brunet, J. Dobson, M. J. Lee, and C. B. Williams, “Microwave Beam Position Monitors”, SLAC TN 64-45, July, 1964 (available from the SLAC Library). See also Martin J. Lee, “The Effect of Rotation of a TM120 Cavity on the Amplitude and Phase of the Beam-Induced Signal”, SLAC TN 64-66, October, 1964 (available from the SLAC Library).

and this energy damps after bunch passage, with e-folding time of $T_f/2 \approx 18.1$ ns ($T_f/2 \approx 34$ ns for Blue Book loaded Q). Peak power radiated is

$$P_w \approx 1.96\frac{U}{T_f} \approx 4.37\times10^{-8}\,\mathrm{W}\left[Q_b(\mathrm{nC})x_b(\mu\mathrm{m})\right]^2,$$

using $\beta \approx 45.2$ and $T_f \approx 36.2$ ns. (For Blue Book loaded Q, the coefficient is $2.9\times10^{-8}\,\mathrm{W}$, or 1.9 dB lower, since single-bunch output is not helped by resonance).

$$10\log_{10}P_w(\mathrm{mW}) \approx -43.6\,\mathrm{dBm} + 20\log_{10}\left[Q_b(\mathrm{nC})x_b(\mu\mathrm{m})\right].$$

For an SLD high-charge bunch of 5 nC (3.1×10^{10} electrons) offset by 1 μm, this provides -30 dBm. For a single bunch of 17.5 pC (1.1×10^{8} electrons) this provides -79 dBm. (As a point of reference, a train of such bunches arriving at 2856MHz corresponds to 50 mA).

For multibunch operation, with a "top-hat" current profile, the "effective charge" is $Q_{eff} = 103.5Q_b$ for $Q_L \approx 325$. ($Q_{eff} = 191Q_b$, for $Q_L \approx 600$). This gives us

$$P_w \approx 5.73\times10^{-11}\,\mathrm{W}\left[I_b(\mathrm{mA})x_b(\mu\mathrm{m})\right]^2, \qquad \Leftrightarrow \qquad 57.3\mu\mathrm{W}/\mathrm{mA}^2\mathrm{mm}^2$$

or

$$10\log_{10}P_w(\mathrm{mW}) \approx -72.4\,\mathrm{dBm} + 20\log_{10}\left[I_b(\mathrm{mA})x_b(\mu\mathrm{m})\right].$$

This corresponds to 57% of the sensitivity quoted in the Blue Book, 100 μW/mA^{2}mm^2. Had we employed $Q_L \approx 600$, the result would agree to 5%. Brunet, *et al.*, list the "experimental sensitivity" 85 μW/mA^{2}mm^2 (their Fig. 12, p. 23).

These estimates assume a tuned cavity, and no phase-drift along the bunh train. For reference, the Blue Book operating temperature is 110°F, fabrication tolerance at 2856 MHz±0.6 MHz (tuning errors from fabrication are at the level of MHz/mil), temperature tuning of 25 kHz/°F. Calculation of transient waveforms can be made using algorithms similar to those indicated for the phase-cavity, recognizing that one has the additional interest in systematics due to $\Sigma \neq \sigma_z$, *i.e.*, field nonlinearities. We observe that it is technically possible, under conditions of 100 μm spot-size, to steer the beam by 0.9 cm in the vertical, thus producing corrections at the 1% level in induced voltage. Such an operational condition would be revealed, however, by the adjacent *y*-BPM, and could be corrected. For nominal conditions, nonlinearities should be negligible.

We wish to employ this mode as an *x*-sensitive pickup, and our concern is resolution. The matter of the time-scale for resolution (jitter versus drift) is still being discussed. Nevertheless let us indicate the general considerations.

One's first thought concerning resolution might be that thermal noise is a limit. This is far from the case, as a simple calculation will show. For comparison, at 112°F (44°C, 318°K) $k_BT \approx 27\,\mathrm{meV} \approx 4.4\times10^{-21}$ J. In a 1 GHz bandwidth one expects 4.4×10^{-12} W or -114 dBm. The natural full bandwidth of the *x*-cavity is $\Delta f = f_0/Q_L \approx 10$ MHz and in this bandwidth the noise power is 4.0×10^{-14} W or -134 dBm. With the latter number, a beam-induced signal will drop into the noise at $Q_{eff}x_b \approx 30\,\mathrm{pC-nm}$ for the linac *x*-cavity.[18]

[18] The figure is 2 pC for the φ–cavity and its 2 MHz bandwidth.

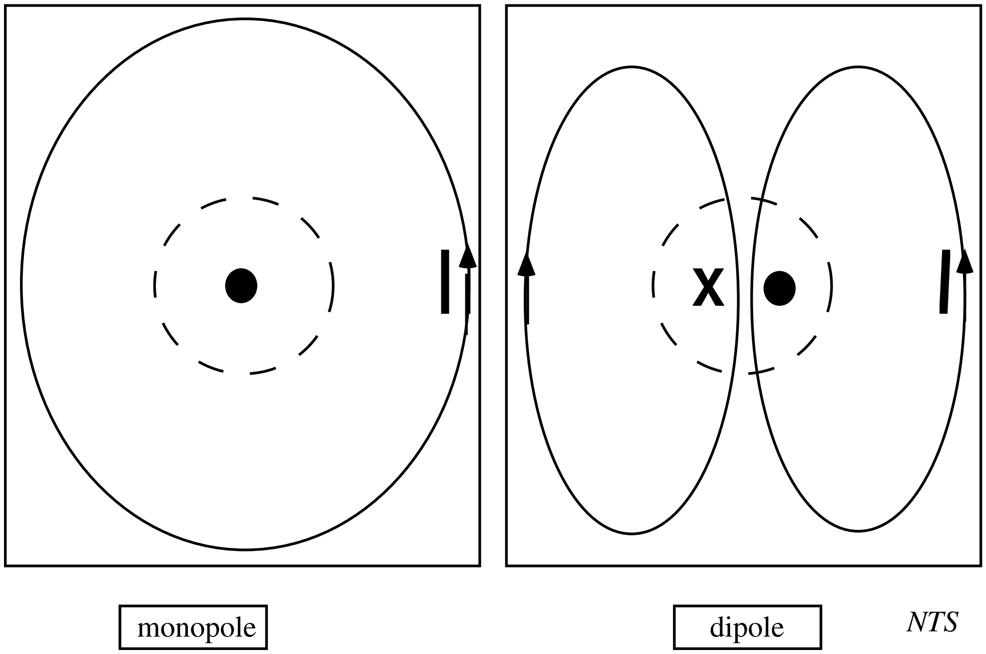

FIGURE 2.10. This cartoon illustrates loop coupling to the two modes. Electric field is indicated by the solid dots and the cross; magnetic field lines correspond to the circles; the beam aperture is indicated by the dotted circle. The coupling loop depicted by the solid bar, enclosed some flux from each mode. As a result, the voltage waveform induced on the output waveguide includes contributions from both modes.

The *x*-cavity output suffers in principle from additional systematics, relating to other modes of the cavity, and the circumstance that dipole output is nominally being used near a centered orbit. Signals induced in other cavity modes become an issue long before the theoretical noise level is reached.[19] At the same time, such effects are in principle susceptible to diminution when differential output is the quantity of interest, particularly on short time scales of minutes, where diurnal drifts in offset are not an issue. While several modes are discussed in the associated technical notes, the primary "common mode" of concern is the 1893 MHz monopole mode, just the perturbed version of the TM110 mode of the closed pillbox. Closed pillbox estimates give $f_M = 1.8875\,\text{GHz}$, $Q_w \approx 1.66 \times 10^4$, $[R/Q] \approx 215\,\Omega$, $k_l \approx 0.64\,\text{V/pC}$, and $R = 3.6\,\text{M}\Omega$ (unloaded). These figures are quite close to the `GdfidL` results: $Q_w \approx 1.72 \times 10^4$, and $[R/Q] \approx 196\,\Omega$. As indicated in Fig. 2.10, this mode should couple quite well to our loop coupler, and thus will in principle show up on our waveforms upstairs. More recent cavity BPM's employed for high-precision work attempt to remove such common mode effects by means of symmetric coupling, as indicated in Fig. 2.11. For E158, for reasons of cost, it is desirable to employ the existing, asymmetric output cavities. Thus the effect of the common mode must be accounted for.

The effect of this common mode depends in detail on the signal handling and the mode of operation. Let us indicate the limits on position resolution, due to this mode, in several different operating schemes. This is dicussion is not intended to put bounds on the cleverness one might try to employ, rather, to indicate what manner of cleverness one must apply. We keep in mind too, though, that clever schemes are usually more complicated, and more difficult to make work.

[19] Environmental noise may be an issue depending on the environment, and the shielding and cabling employed for the pickups and electronics.

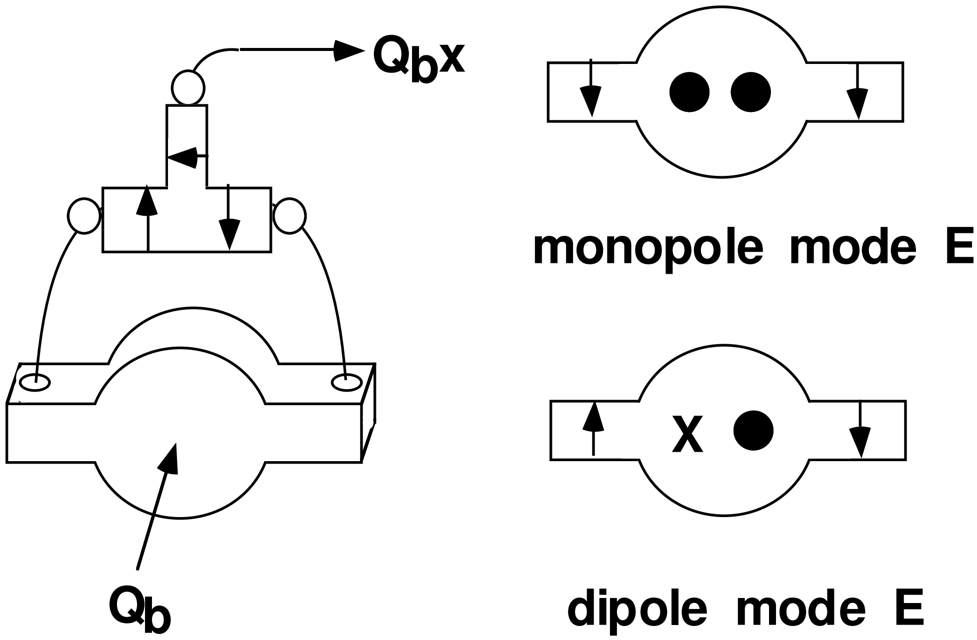

FIGURE 2.11. To illustrate that with symmetric couplers and a hybrid ("magic") tee, and carefully chosen guide lengths one can separate modes of opposite symmetry. Isolation of 25 dB is considered not hard.

First, let us consider the single-bunch mode of operation. Single-bunch mode operation is interesting because this mode is available during SLC running for pre-E158 tests; conditions would preferably be only e^- to sector 30 and low charge (to simplify accurate orbit analysis in the linac). Let us ask what our expectations are under such conditions, as these inform the question of what tests are useful to perform.

Suppose in the simplest (and worst) case, that one performs power detection on the unfiltered output of the x-cavity signal. Assuming comparable guide-couplings for the modes, one may estimate the position resolution by equating the energy deposited in the dipole mode with that in the monopole mode $U_d = k_\perp (Q_b x_b)^2 = U_m = k_l Q_b^2$. Using $k_l \approx 0.64\,\mathrm{V/pC}$ and $k_\perp \approx 8.07\times10^{-2}\ V/\mathrm{pC}-\mathrm{cm}^2$, one can see that these are equal at the (unphysical) value $x_b \approx 2.8\,\mathrm{cm}$! Not liking this very much, let's consider filtering followed by power detection. We suppose a very sharply cut-off high-pass filter (a piece of cut-off waveguide, for example). In this case, we are samping the high-frequency tail of a Lorentzian response function and the received voltage amplitude from the common mode is reduced by a factor of $1/Q_L$. In this case, common mode and dipole mode signals become comparable in amplitude at offsets on the order of $x_b \approx 2.8\,\mathrm{cm}/600 \approx O(50\,\mu\mathrm{m})$. This is typical, for example, of the kind of resolution one obtains looking at the dipole-mode output of a linac accelerating structure, employing high-pass filtering to block the monopole mode.

If in addition, by means of symmetric output coupling we were able to subtract out the symmetric mode, so that the voltage picked up took the form $V_d + \varepsilon V_m$, then our position resolution would be $x_b \approx O(50\,\mu\mathrm{m})\varepsilon$. With a hybrid ("magic") tee, 25 dB of isolation would be considered not hard, and this corresponds to $\varepsilon \approx 6\times10^{-2}$, and $x_b \approx O(3\,\mu\mathrm{m})$. None of these considerations consulted the charge of the bunch; they do assume however that it is a point bunch, and not a bunch train.[20]

Let us consider next the situation for a bunched beam driving such a mode off resonance. This is the case of operational interest. Excitation of a mode off-resonance has been calculated in a previous note, and the relevant figure of merit is

$$\eta \approx \frac{1}{2}\frac{1}{\sqrt{\sin^2\left(\pi\Omega/\Omega_0\right)+\left(\pi\Omega/2\Omega_0 Q_L\right)^2}},$$

for a mode with (damping-corrected) resonant angular frequency Ω_0, and loaded Q, Q_L, driven by a beam bunched at angular frequency Ω_0. This is to be compared to Q_{L0}/π for the design mode.The argument of the sine function for the common mode of the linac cavity is 119°, so that $\eta \approx 0.6$. This is to say that destructive interference is such that the steady-state amplitude in the common mode is equivalent to the amplitude produced by one single bunch with $0.6\times$ the nominal single bunch charge. Meanwhile, for the design mode $Q_{L0}/\pi \approx 100$. In this case, to compare common-mode and dipole-mode signals, we should compare $k_\perp\left(Q_{beff}x_b\right)^2$ and $k_l Q_b^2\eta^2$, and we obtain $x_b \approx O\left(2\times10^2\ \mu\text{m}\right)$.

Now, however, filtering doesn't help, since the signal we are considering is a driven oscillation at the beam frequency. With symmetrized output coupling, and a tee with isolation of 25 dB, we can bring this estimate to $x_b \approx O(10\,\mu\text{m})$. If critical coupling had been employed ($Q_e = Q_w = 2Q_L$) we would have $Q_L \approx 7.5\times10^3$, corresponding to $Q_{beff} = 2.4\times10^3 Q_b$, and resolution approaching $x_b \approx O(10\ \mu\text{m})$, without symmetric coupling. Iin this case, with symmetric coupling and 25 dB of isolation we would have $x_b \approx O(0.5\ \mu\text{m})$. This is the ultimate resolution of any S-Band structure employing straight-power detection.

Power detection, however, is only the crudest possibility. The foregoing discussion was based on comparison of signal power levels; this generally leads to somewhat too pessimistic an answer. The mere presence of an offset in a signal does not imply that one cannot detect small changes in the total signal. More is available to us in the way of information than just the amplitude of the emitted signal. We can employ phase-information. With reliable phase information, such as one expects to be provided by the φ-cavity, it is possible in principle to perform vector subtraction to remove the common mode. This may be illustrated most simply referring to the "baseband integral" of the down-mixed waveform corresponding to the common mode,

$$\int_{-\infty}^{+\infty} dt\, \tilde{V}_c(t) e^{j\Delta\Omega(t-T)} \approx \frac{R_L Q_b}{1-jT_f\Delta\Omega},$$

with $R_L = Q_L[R/Q]$ the loaded shunt impedance of the common mode, and $\Delta\Omega = \Omega - \Omega_0$ the detuning from resonance. Taking $\Omega \approx 2\pi\times1.89\,\text{GHz}$ and $\Omega_0 \approx 2\pi\times2.856\,\text{GHz}$, with $T_f \approx 100\,\text{ns}$, one has $T_f\Delta\Omega \approx 6.1\times10^2$, in agreement with the foregoing estimates based on the figure of merit, η. The feature to note about this result is that the phase of this signal is fixed with respect to the beam, and independent of offset. Thus if a reliable phase-reference is available upstairs (for example the phase-cavity signal itself), the signal can be balanced out in a tee. The idea fails if for any reason the common mode phase or amplitude drift appreciably with respect to

[20] We could add, in passing, that an alternative to filtering employed by Shintake [ref], consists of designing a cavity a heavily de-Q'd common mode, and gating the output waveform well after the evanescence of the monopole mode.

the reference signal, over the measurement interval (minutes, hours or days, to be determined). A sketch of the idea is seen in Fig. 2.12. The idea relies on the assumption that the driven oscillation in the common mode as seen upstairs has an amplitude and phase fixed in relation to the monopole mode of the phase cavity. Assuming the same cable runs, and equal cable lengths, this may be achievable in a diurnally-reliable fashion. In the case that consistent monitoring is required only over the scale only of minutes it seems even more promising. The phase-shifter and attenuator would require initial adjustment (frequent adjustment if diurnal issues appear). The shortest procedure for adjustment would be to adjust the phase-shifter and attenuator to zero the output of the tee. Maximum sensitivity to position would then be available at whatever the current location of the beam. One could devise an iterative procedure to center the beam accurately (as opposed to monitoring changes accurately) and we leave this to a later note. This idea requires further analysis; it appears that it could be tested using the LI30 BPM.

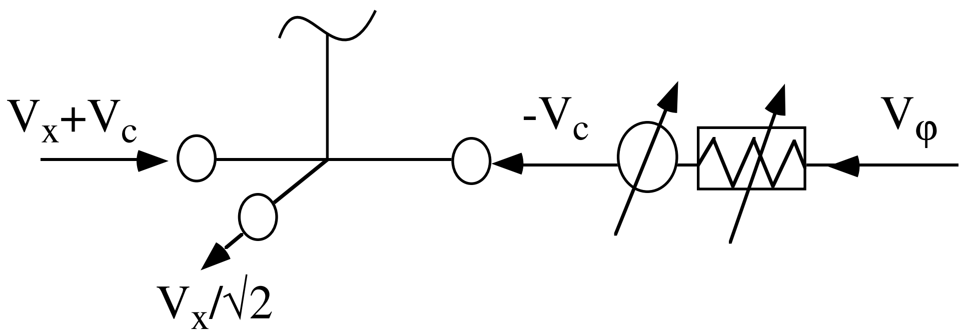

FIGURE 2.12 In principle one may subtract out a steady common mode signal, by making use of the phase-cavity signal and a magic tee.

Let us conclude this discussion with a potpourri of some minor features we would like to dismiss. In the BPM cavity there is also a *y*-sensitive mode, the TM120 mode, with fields given by wall Q is $Q_w \approx 1.82 \times 10^4$ Loss factor is $k_\perp \approx 1.17 \times 10^{-1}\ V/\mathrm{pC-cm}^2$, about 40% larger than for the TM210 mode, due to the fact that the *y*-dimension of the cavity is smaller. Given the expected poor external coupling of this mode, we may suppose that the loaded Q of the mode is just the wall Q. The natural field decrement time of the mode is then $T_0 = 2Q_w/\omega \approx 1.88\,\mu\mathrm{s}$, and one may expect a voltage below that for resonant response by a factor of $\Delta\Omega T_0 \approx 2\pi \times 232\,\mathrm{MHz} \times 1.88\,\mu\mathrm{s} \approx 2.7 \times 10^3$. This together with the absence of good coupling suggests that this mode is of no particular concern.

One additional *y*-dipole mode is noteworthy in that it is located rather close to the $3 \times 2856\ \mathrm{MHz} = 8568\ \mathrm{MHz}$ beam harmonic. This is mode #35, at 8592 MHz (GdfidL), with $\left[R_\perp/Q\right] \approx 0.7\ \Omega\mathrm{cm}^{-2}$. This mode couples poorly, and is most likely detuned from resonance.

An additional effect one should check is the effect on the beam of the cavities employed as pickups. For the φ-cavity, bunches will experience a retarding voltage on the order of $V \approx R_L I_b \equiv 2k_l Q_{eq}$. Using $R_L \approx 0.3\ \mathrm{M}\Omega$, this corresponds to 30 kV/100 mA of beam current, not a significant effect. The position cavities also act back on the beam, providing a transverse kick. The amplitude of the sinusoidal kick function may be expressed as

$$\Delta x' \approx \frac{e}{mc\gamma} R_{\perp L} I_b x_b^2,$$

Using $R_{\perp L} \approx 5.4 \times 10^3\ \Omega/\mathrm{cm}^2$, and 45 GeV for the beam energy, this amounts to 1×10^{-12}rad/ 100 mA for a 100 μm beam offset. Actual deflection experienced by a bunch is reduced by an additional factor of order $\Omega\sigma_t \approx 10^{-2}$, arising from the 90° phase-lag between electric and magnetic fields. This is a very small effect and can be ignored.

2.3 Network Analysis, Now and Later

Cable employed at present, and its specs, need to be checked to estimate cable attenuation, and to insure that fundamental mode guide is used. All cavities, cables and connectors should then be visually inspected at a minimum. Presence of pulsed devices in the vicinity of any cable should be noted. Status of LCW hookup should be noted, and presence or absence of temperature monitors on each cavity should be noted. Once the decision as to choice and location of cavities is made, LCW hookup and temperature monitors will be required where missing. It is possible that new cable may be required. A later note will report the outcome of this work.

Lengths of cable subject to diurnal temperature variation should be of roughly equal length. Recall that expansion ΔL of a length L is given by $\Delta L / L = \alpha \Delta T$, with α the thermal coefficient of expansion. So for example, for copper, $\alpha \approx 1.7 \times 10^{-5} / °\mathrm{C}$. Thus if one has a 100' cable run subject to a day-night temperature variation of 40°F (22°C), one may expect cable lengths to vary on the order of 1.15 cm [correct this for actual cable employed]. Net phase-shift through the cable is then 40°. However, if the cables are of exactly equal length and subject to the same temperature variation, then this phase-shift is of no consequence. (To be sure, if one is using an MDL-derived phase-reference, it would cause problems, but we are eschewing direct use of MDL phase-derived information). If the cable lengths differ by 1', then the phase variation is 0.4°, and this is probably acceptable. Cable lengths can be checked by time-domain reflectometry, for example. At a more mundane level, one may expect to find perhaps that some cables are damaged, disconnected, things like that, so a check of the network is a must.

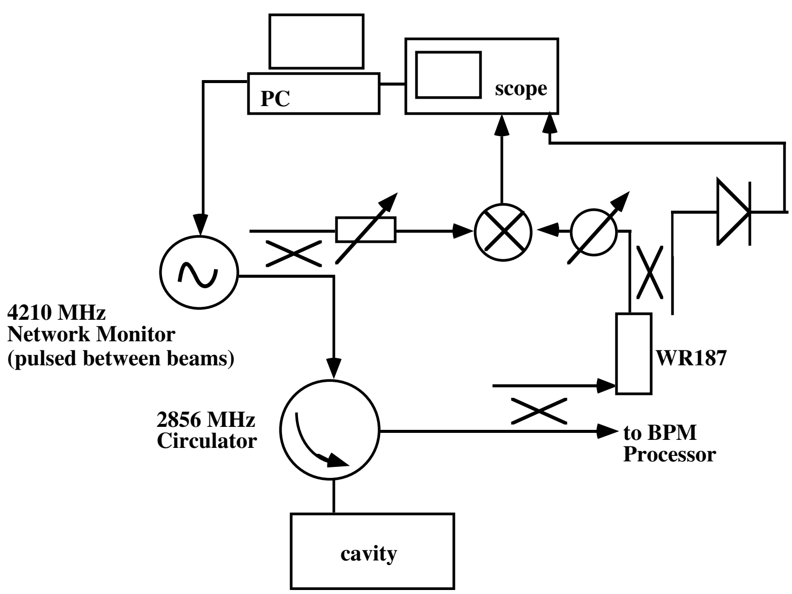

FIGURE 2.13 Setup for network analysis with beam-on.

Along the same lines, but a higher level of refinement, S_{11} looking down the cable into the cavity can be measured from upstairs, with an S-Band network analyzer, absent beam. One shouldn't get too elaborate with this until LCW hookup and temperature stabilization is confirmed;

measurement should be performed with the cavity at temperature and under vacuum. Assuming systematics of cable reflections are not a nuisance, cavity tune can be confirmed in this way. An insitu off-beam cavity probe can also be contemplated for use during operation as a means of insuring accurate cavity tune; for this however, systematic effects from cable mismatches and thermal expansion need to be dealt with. This concept is illustrated in Fig. 2.13.

While we are discussing the matter of the network, let us digress to recall the particulars of S_{11} measurement on a cavity connected to a guide. It is conventional to characterize the difference in drive frequency ω from the resonant frequency ω_0 of the cavity by the *tuning angle* ψ,

$$\tan\psi = Q_L\left(\frac{\omega_0}{\omega} - \frac{\omega}{\omega_0}\right),$$

and this definition is more precise than the one employed above, although the difference is negligible for our high Q cavity. In terms of tuning angle, in steady-state, driving a forward voltage phasor $\tilde{V}_F$ down the guide toward the cavity, the cavity voltage is

$$\tilde{V}_c = \frac{2\beta}{1+\beta}\cos\psi e^{j\psi}\tilde{V}_F.$$

Notice that tuning angle is the angle the cavity voltage phasor $\tilde{V}_C$ makes with the forward drive phasor $\tilde{V}_F$. On resonance, the two are in phase,

$$\tilde{V}_C = \frac{2\beta}{1+\beta}\tilde{V}_F, \qquad (\psi = 0 \Leftrightarrow \omega = \omega_0 \Leftrightarrow resonance)$$

and a reflected signal is propagating back up the waveguide toward the source,

$$\tilde{V}_R = \tilde{V}_C - \tilde{V}_F = \frac{\beta - 1}{\beta + 1}\tilde{V}_F. \qquad (\psi = 0 \Leftrightarrow \omega = \omega_0 \Leftrightarrow resonance)$$

If β>1 the external Q is lower than the wall Q, and the cavity is said to be *over-coupled*. In this case the reflected signal is in phase with the forward drive. If β<1 the cavity is said to be *under-coupled* and in this case the reflected signal is 180° out of phase with the drive. If β=1 the cavity is said to be *critically-coupled*, and there is no reflected signal in steady-state. For the phase-cavity the steady-state reflection coefficient on resonance is 0.75, *i.e.*, 56% (-2.5 dB) of the power incident on the cavity is reflected (the rest is absorbed in the cavity walls).

With this result for cavity voltage, we may compute the reflection coefficient using the continuity condition, $\tilde{V}_R = \tilde{V}_c - \tilde{V}_F$,

$$S_{11} = \frac{\tilde{V}_R}{\tilde{V}_F} = \frac{2\beta}{1+\beta}\cos\psi e^{j\psi} - 1.$$

Notice that measurement of the (complex) S-matrix can permit one to determine the resonant frequency ω_0, the coupling factor β, and the loaded Q. Thus one can extract as well the external Q. Once these are measured with the cavities under vacuum and temperature-stable conditions, the network analyzer could be removed, and simpler scheme employing a frequency-sweeping signal generator could be employed for monitoring of the network, something like that depicted in Fig.

5.1 (Sec. 5), sweeping frequency and confirming the expected S_{11}. To protect equipment it would be easiest to monitor a higher mode, and employ cutoff guide to block the high power S-Band signals induced by the beam.[21]

[21] This is similar to the technique employed in the work of David Pritzkau, *et al.,* in their pulsed heating studies (see ARDB Technical Note Library).

3. Idealized Signal Processing

3.1 Generica Baseband Waveforms

In this section we examine in more detail the systematics involved in the processing of the waveforms we have computed. [This analysis is not compete as of this revision] Most simply we can express the voltage phasors from the position and phase cavities, as they would appear upstairs after front-end processing (down-mixing) as

$$\tilde{V}_x = c_x Q_{eff} x + \varepsilon_x Q_{eff}, \qquad \tilde{V}_\varphi = c_\varphi Q_{eff} e^{j\phi}.$$

The term ε_x represents the common mode component. The phase ϕ we introduce to account for any phase-error incurred in the signal processing (e.g., differential cable expansion or down-mixing with an LO that has drifted in phase from the nominal value). The coefficients c_x, c_φ are determined from calculations in the foregoing sections, and cable propagation characteristics. The effective charge Q_{eff}, is determined from the convolution of beam current with the cavity response, and includes in it a choice of sampling technique (peak sample, gated integration, etc.). We can express the position phasor as

$$\tilde{V}_x = c_x Q_{eff} \left(x - \tilde{x}_0 \right),$$

where the offset

$$\tilde{x}_0 = -\frac{\varepsilon_x}{c_x} = x_{0r} + jx_{oi},$$

is in general complex. Dependence of voltage amplitude on position is given by

$$\left|\tilde{V}_x\right|^2 = \left|c_x Q_{eff}\right|^2 \left\{ \left(x - x_{0r}\right)^2 + x_{oi}^2 \right\},$$

and exhibits both a non-zero minimum and an offset from the center-axis defined by the position-sensitive mode.

For a phase-sensitive measurement, inferred position will take the form

$$X = k \Re \frac{\tilde{V}_x \tilde{V}_\varphi^*}{\tilde{V}_\varphi \tilde{V}_\varphi^*} = k \Re \frac{\left(c_x x + \varepsilon_x\right)}{c_\varphi e^{j\phi}} = Sx + X_0,$$

with some choice of scale calibration constant k. Thus the response of such a BPM is determined from the scale, and the offset,

$$S = k \Re \frac{c_x}{c_\varphi} e^{-j\phi}, \qquad \text{(BPM scale factor)}$$

$$X_0 = k \Re \frac{\varepsilon_x}{c_\varphi} e^{-j\phi}. \qquad \text{(BPM offset)}$$

3.2 Scale & Offset

Next let us analyze the systematic errors in offset and scale, to characterize the intrinsic resolution of the BPM. To do so in the most specific fashion, we should indicate by what means the voltage phasors are processed. The basic choices are: peak detection or gated integration. For simplicity, we will assume that the full voltage waveforms are integrated (gate with gatewidth longer than the pulse length). There is in fact a potentially strong reason for considering this manner of detection, namely that the area under the cavity phasor curve is proportional to the pulse-averaged charge (in the case of $\int \tilde{V}_\varphi dt$) or the pulse-averaged, charge-weighted position (in the case of $\int \tilde{V}_x dt$). Such integrals are just the area under the scope waveform obtained by mixing down to baseband and easily amenable to acquisition.

Thus we choose to identify,

$$\tilde{V}_\varphi \equiv e^{j\phi} \int_{-\infty}^{+\infty} dt\, \tilde{V}_{\varphi c}(t) \approx e^{j\phi} R_L \sum_n Q_{bn} \exp\left(-\tfrac{1}{2}\beta_0^2 \sigma_{zn}^2\right),$$

$$\tilde{V}_x \equiv \int_{-\infty}^{+\infty} dt\, \tilde{V}_{xC}(t) \approx R_{\perp L} \sum_n Q_{bn} x_b \exp\left(-\tfrac{1}{2}k_0^2 \Sigma_{xn}^2\right) + n''\eta \frac{R_{L-CM}}{1 - jT_f \Delta\Omega} \sum_n Q_{bn} \exp\left(-\tfrac{1}{2}k_0^2 \Sigma_{cn}^2\right).$$

The impedance transformation factor is $n'' \approx 0.30\,\text{cm}^{-1}$, as discussed in TN153. The factor $\exp\left(-\tfrac{1}{2}\beta_0^2 \Sigma_{cn}^2\right)$ is the generalized form factor for the common mode, and includes a right quadrupole component. In the last expression, we include a factor η to account for any cleverness employed against the common mode. From these expressions we may identify (neglecting cable propagation factors)

$$c_\varphi Q_{eff} \approx R_L \sum_n Q_{bn} \exp\left(-\tfrac{1}{2}k_0^2 \sigma_{zn}^2\right),$$
$$c_x Q_{eff} x \approx R_{\perp L} \sum_n Q_{bn} x_b \exp\left(-\tfrac{1}{2}k_0^2 \Sigma_{xn}^2\right),$$
$$\varepsilon_x Q_{eff} \approx n''\eta \frac{R_{L-CM}}{1 - jT_f \Delta\Omega} \sum_n Q_{bn} \exp\left(-\tfrac{1}{2}k_0^2 \Sigma_{cn}^2\right).$$

Scaled position readout is then given by

$$Sx = k \frac{R_{\perp L}}{R_L} \frac{\sum_n Q_{bn} x_{bn} \exp\left(-\tfrac{1}{2}k_0^2 \Sigma_{xn}^2\right)}{\sum_n Q_{bn} \exp\left(-\tfrac{1}{2}k_0^2 \sigma_{zn}^2\right)} \cos\phi,$$

or,

$$S = k \frac{R_{\perp L}}{R_L} \frac{\sum_n Q_{bn} x_{bn} \exp\left(-\tfrac{1}{2}k_0^2 \Sigma_{xn}^2\right)}{\sum_n Q_{bn} \exp\left(-\tfrac{1}{2}k_0^2 \sigma_{zn}^2\right)} \frac{\sum_n Q_{bn}}{\sum_n Q_{bn} x_{bn}} \cos\phi,$$

where we introduce the actual charge-weighted beam-centroid

$$x \equiv \frac{\sum_n Q_{bn} x_{bn}}{\sum_n Q_{bn}}.$$

Offset is given by

$$X_0 \approx k\,n''\eta \frac{R_{L-CM}}{R_L} \frac{\sum_n Q_{bn} \exp\left(-\tfrac{1}{2}\beta_0^2\,\Sigma_{cn}^2\right)}{\sum_n Q_{bn} \exp\left(-\tfrac{1}{2}k_0^2\,\sigma_{zn}^2\right)} \Re \frac{e^{-j\phi}}{1 - j\,T_f \Delta\Omega}$$

$$\approx k\,n''\eta \frac{R_{L-CM}}{R_L} \frac{\sum_n Q_{bn} \exp\left(-\tfrac{1}{2}\beta_0^2\,\Sigma_{cn}^2\right)}{\sum_n Q_{bn} \exp\left(-\tfrac{1}{2}k_0^2\,\sigma_{zn}^2\right)} \cos(\psi - \phi)\cos\psi,$$

where we express the detuning of the beam from the common mode resonance in terms of $\tan\psi = T_f \Delta\Omega$. We may simplify this expression somewhat to read

$$X_0 \approx k\,n''\eta \frac{R_{L-CM}}{R_L} \frac{\sum_n Q_{bn} \exp\left(-\tfrac{1}{2}\beta_0^2\,\Sigma_{cn}^2\right)}{\sum_n Q_{bn} \exp\left(-\tfrac{1}{2}\beta_0^2\,\sigma_{zn}^2\right)} \frac{\sin\phi}{\Delta\Omega T_f}.$$

In the case of small form factor correction, and negligible common mode one has

$$S = k \frac{R_{\perp L}}{R_L} \cos\phi.$$

Supposing that the calibration factor $k = R_L / R_{\perp L}$ is chosen to make this unity, for $\cos\phi = 1$, we have then in general,

$$S = \frac{\sum_n Q_{bn} x_{bn} \exp\left(-\tfrac{1}{2}k_0^2\,\Sigma_{xn}^2\right)}{\sum_n Q_{bn} \exp\left(-\tfrac{1}{2}k_0^2\,\sigma_{zn}^2\right)} \frac{\sum_n Q_{bn}}{\sum_n Q_{bn} x_{bn}} \cos\phi.$$

The offset is

$$X_0 \approx \eta\, n'' \frac{R_{L-CM}}{R_{\perp L}} \frac{\sum_n Q_{bn} \exp\left(-\tfrac{1}{2}\beta_0^2\,\Sigma_{cn}^2\right)}{\sum_n Q_{bn} \exp\left(-\tfrac{1}{2}\beta_0^2\,\sigma_{zn}^2\right)} \frac{\sin\phi}{\Delta\Omega T_f}.$$

Notice that a priori, the definition employed for x leaves one subject to variation within the pulse of centroid position. One could in principle find x=0, when in fact the head is at +100 μm, and the tail is at -100 μm. This suggest that analysis of time resolved position data will eventually be required. We put this aside for now.

To resolve 1 μm out of 100 μm, we must insure that the scale factor is constant at the level of 1%. The simplest estimate, for a "top-hat" macropulse with no chirp in beam variables, is

$$S \approx \left\{1 + \varepsilon_{NS}\left(x_b^2 - 3y_b^2 + 3\sigma_x^2 - 3\sigma_y^2\right)\right\}\cos\phi ,$$

with no bunch length dependence. Recall that $\varepsilon_{NS} = -4.2 \times 10^{-3}\,\mathrm{cm}^{-2}$ is small, with the result that scale deviation due to nonlinearities occurs only for gross vertical misteering, 0.9 cm. We require that ϕ be stable to better than 8°. Reliable scale factor seems not to be a challenge in principle.

We must also insure that the offset is stable to 1 μm over the measurement period (minutes, hours or days---to be determined). This is the point where we become very interested in the quadrupolar content of the 1.88 GHz mode of the *x*-cavity. In a previous note we found that a predominantly monopolar mode of an asymmetric cavity has leading order multipole correction quantifiable in the form,

$$\Sigma^2 \approx \sigma_z^2 - \frac{2}{k_0^2}\varepsilon_{NQ}\left(x_b^2 - y_b^2 + \sigma_x^2 - \sigma_y^2\right).$$

The normal quad component ε_{NQ} for the common mode of the linac-style *x*-cavity was evaluated with the field-solver `GdfidL` and found to be $\varepsilon_{NQ} \approx 6.3 \times 10^{-3}\,\mathrm{cm}^{-2}$, thus the dimensionless coefficient $2\varepsilon_{NQ}/k_0^2 \approx 3.5 \times 10^{-2}$. As a consequence of this quadrupolear component in the common-mode, the offset takes on a dependence on beam-coordinates.

$$X_0 \approx X_0\left(\vec{r}_\perp = 0\right)\left\{1 + \varepsilon_{NQ}\left(x_b^2 - y_b^2 + \sigma_x^2 - \sigma_y^2\right)\right\}.$$

So, for example, let us suppose that operation with a beam motion over a range as large as $x_b \approx 1$ mm is envisioned, and, at the same time it is required that the offset remain stable at the level of 1 μm. In this case we require,

$$X_0\left(\vec{r}_\perp = 0\right) \times 6.3 \times 10^{-3}\,\mathrm{cm}^{-2} \times \left(0.1\,\mathrm{cm}\right)^2 < 1\,\mu\mathrm{m},$$

or

$$X_0 < 1.6\ \mathrm{cm}.$$

Thus the absolute "fictitious" offset X_0 cannot be too large. We can estimate its magnitude using

$$n'' = \left(Q_{ed}\left[R_{\perp d}/Q\right]\right)^{1/2} / \left(Q_{eCM}\left[R_{CM}/Q\right]\right)^{1/2} \approx 0.30\ \mathrm{cm}^{-1},$$
$$R_{L-CM} = Q_L\left[R/Q\right] \approx 600 \times 196\ \Omega \approx 0.12\ \mathrm{M}\Omega,$$
$$R_{\perp L} = Q_L\left[R_\perp/Q\right] \approx 300 \times 17.8\ \Omega\mathrm{cm}^{-2} \approx 5.3\ \mathrm{k}\Omega\mathrm{cm}^{-2},$$

and $T_f\Delta\Omega \approx 6.1 \times 10^2$. We find

$$X_0 \approx \eta n'' \frac{R_{L-CM}}{R_{\perp L}} \frac{\sin\phi}{\Delta\Omega T_f} \approx 1.1\times 10^2\,\mu\text{m}\times\eta\sin\phi .$$

This implies that despite the transverse variation in the common mode, and its possible effect in "faking" beam motion, one has about an order of magnitude to spare.

We will continue this section in later revisions. We put a reminder here that if it should prove necessary to perform common mode subtraction "downstairs" (referred to as symmetrization in other parts of these notes), and should it prove inconvenient, mechanically to pair x-cavities for this purpose, one could employ existing x-y cavity pairs, to provide a single monitor signal (of coordinate in a rotated plane) with lowest order (monopolar) common mode subtracted. We might feel comfortable doing this now that we see the quadrupolar term is small.

Note also that in the case of a macropulse-integrated signal, the effect of equal x-cavity and φ-cavity tuning errors cancel in their contribution to scale-error. That is to say that both phasors are multiplied by the same complex correction factor $\cos\psi e^{j\psi}$, and these factors cancel. The residual effect of cavity tuning error in this case is through the offset X_0. The common mode, being already greatly detuned, picks up little in the way of a correction in this case. Thus a drift in cavity tune from zero tuning angle to $\delta\psi$, corresponds to results in a different offset, through the normalization signal,

$$X_0 \approx 1.1\times 10^2\,\mu\text{m}\times\eta\frac{\sin(\phi+\delta\psi)}{\cos(\delta\psi)}.$$

To hold offset drift to $1\,\mu\text{m}$ requires, in the worst case, tuning to 0.5°, or about 0.5° F.

4. Front-End BPM Electronics

4.1 *The Simplest Module*

As a “straw-man”, note that the simplest electronics one could employ to monitor position would appear as depicted in Fig. 4.1. This is adequate as is to produce several counts on a LeCroy 2249A GADC at -20 dBm input power levels. Notice that the phase-signal isn’t used; normalization could be performed with the toroid signal. Each diode should be employed in the linear regime, else the added complication of diode polynomials would be required. The variable attenuators need to be reset when charge is varied significantly or significant steering is to be expected. Beam misteering in this configuration could destroy the detector, requiring replacement. Cost for this setup is about $300 per detector, and $2500 per 12 channel GADC. For 5 BPM units, the cost would be about $5500 total; prudence suggests an additional $6000 for replacement diodes. It takes about 1/2 hour to calibrate a diode. Given our power level estimates,

$$10\log_{10} P_w(\mathrm{mW}) \approx -72.4\,\mathrm{dBm} + 20\log_{10}\left[I_b(\mathrm{mA})x_b(\mu\mathrm{m})\right]$$

this system would be adequate to detect a O(5 µm) offsets at 100 mA beam current, at the level of a few counts, provided vector subtraction is performed on the common mode. (This implies still more components not depicted in Fig. 4.1) However, note that with power detection one does not know the sign of the beam offset, and thus use of this signal for steering is frustrated (particularly algorithmic steering as in a feedback loop).

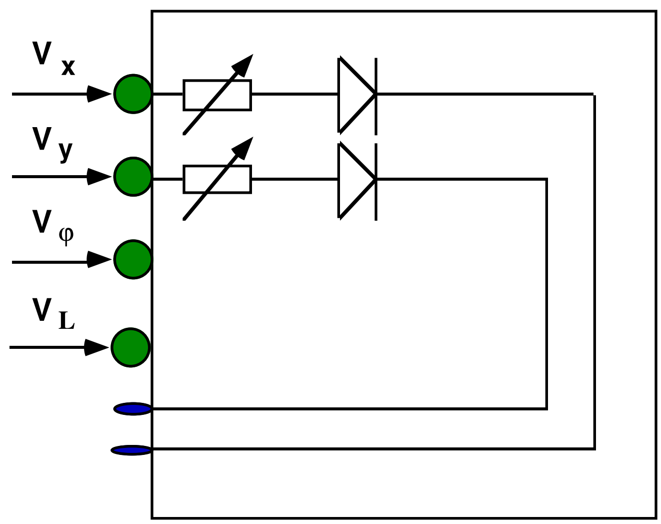

FIGURE 4.1 Simplest electronics for monitoring of beam position.

4.2 *Recommended Front-End*

A more versatile version of a front-end processor is depicted in Fig. 4.2. Regardless of the final electronics decided on, this would be a handy unit to have available during commissioning. It employs isolators to prevent a reflected signal going back down the line to the cavity. (These are not necessary if the line attenuation is large; on the other hand, one would prefer to be using cable where the attenuation is not large). These are followed by variable attenuators; it would be more convenient to have a front-panel adjustment for these, but more liable to misadjustment by passersby. (A pull-down plexiglass shield would be helpful for the front panel.) The variable attenuators are followed by variable phase-shifters. After this, 10 or 20 dB couplers permit front panel monitoring of the raw signal (during commissioning or other debugging). The two position signals are then followed by limiters to protect the expensive IQ (dual output) mixers that follow. The phase signal does not require a limiter, since it will be of relatively constant amplitude, and thus can be attenuated by a large, fixed amount in advance. The frequency for the LO would be the 2856 MHz fundamental and the LO in this configuration could be free-running. The IQ outputs would consist of six pulsed, bipolar video signals. These would most naturally be taken to a track & hold module. Position can be deconvolved according to

$$X = \frac{\tilde{V}_x \tilde{V}_\varphi^*}{\tilde{V}_\varphi \tilde{V}_\varphi^*}.$$

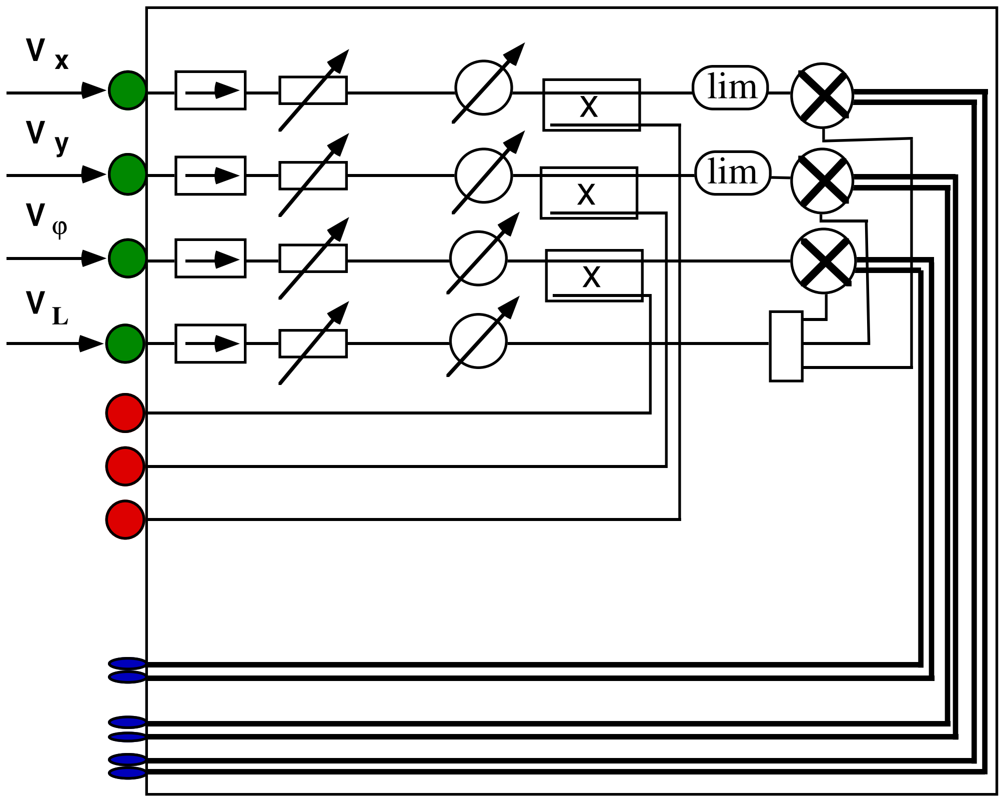

FIGURE 4.2 More versatile front-end processor for the BPM signals.

where we depict the position IQ outputs as the real and imaginary parts of a position phasor $\tilde{V}_x = c_x Q X e^{j\varphi_B - j\varphi_L + j\Delta\phi_x}$, and the phase IQ outputs as the real and imaginary parts of $\tilde{V}_\varphi = c_\varphi Q e^{j\varphi_B - j\varphi_L + j\Delta\phi_\varphi}$.[22] The function of the in-line phase-shifters is to insure that $\Delta\phi_x = \Delta\phi_\varphi$.

A production version of this system would likely modularize the functions, making use of a single version of a box as depicted in Fig.4.3. There would be three such boxes for each BPM station, as indicated in Fig. 4.4 (a) and (b), and fifteen total for 5 BPM stations, plus spares. The advantage of this division into separate modules is in the assembly of the boxes, and the lower cost

[22] Notice that if one didn't feel that the sign of the beam offset was important, one could make do with $|X| = \sqrt{V_{xI}^2 + V_{xQ}^2} / \sqrt{V_{\varphi I}^2 + V_{\varphi Q}^2}$, and a less elaborate setup, since in this case, phase is not an issue. (In this case, one would probably employ crystals).

of spares in the event of failure (destruction of the limiter and/or mixer). As can be seen, comparing, (a) and (b) a choice remains on the digitization scheme, and cost will enter the considerations. Layout (a) requires 15 T&H units ; layout (b) requires only 3 GADC's, and a BNC Model No. 8010 gate generator (or equivalent, not shown, likely could be scavenged).

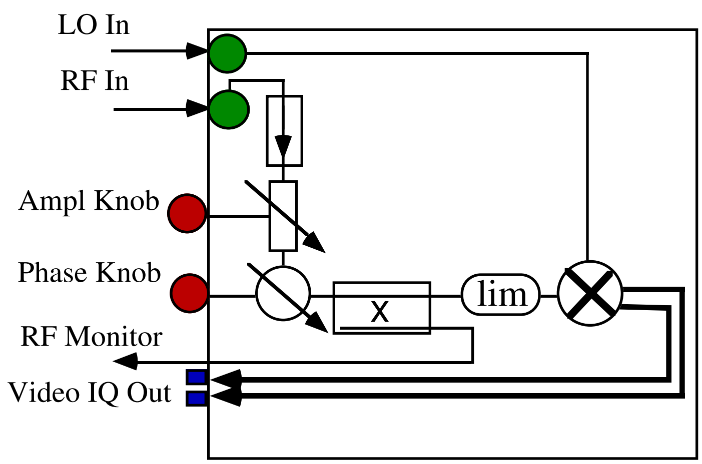

FIGURE 4.3 Modular version of the electronics depicted in Fig. 4.2.

It should be added that these depictions assume the position signals are of sufficient amplitude for the track and hold. [More on T&H] If this is not the case, one may wish to add a low-noise amplifier in front of each mixer. Dynamic range is an issue that remains to be evaluated. On this note, an alternate version of this box would employ a free-running LO at $f_L = f_{2856} + f_{IF}$, use single output mixers to produce IF signals at $f_{IF} \approx 100$ MHz. These could then be processed (filtered, amplified, IQ mixed) using a second LO at f_{IF}. This would lower the cost of the unit, in that the lower frequency components are less expensive. This LO could be free-running, in principle, however, if the high-frequency LO is provided by a modern synthesizing signal generator, it could be phase-locked with the low-frequency LO (by feeding a 100 MHz phase-reference to the back panel).

We don't recommend it, but this system could be further simplified if one is willing to trust phases traceable to the master oscillator. In this case one has 119 MHz available, and multiples of, for example, 4 (476 MHz) and 24 (2856 MHz).

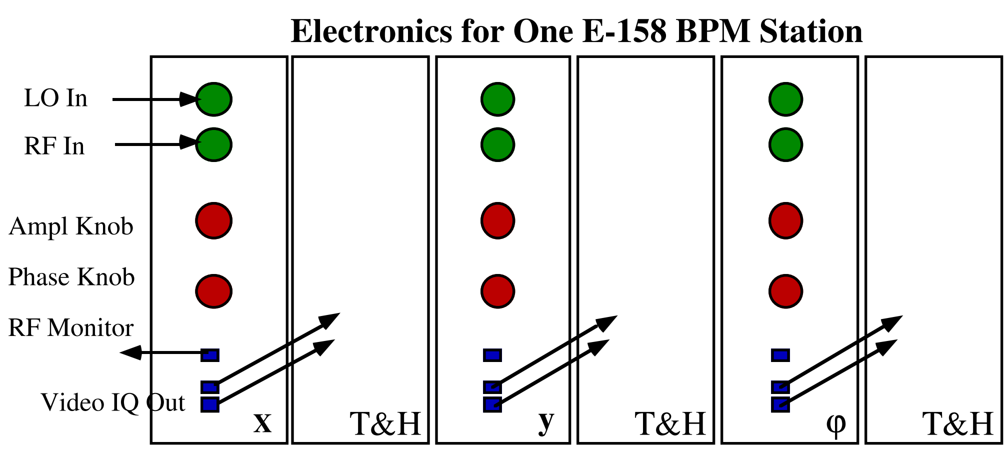

FIGURE 4.4 (a) Electronics for one BPM Station employing the Ni (two-channel) Track & Hold unit.

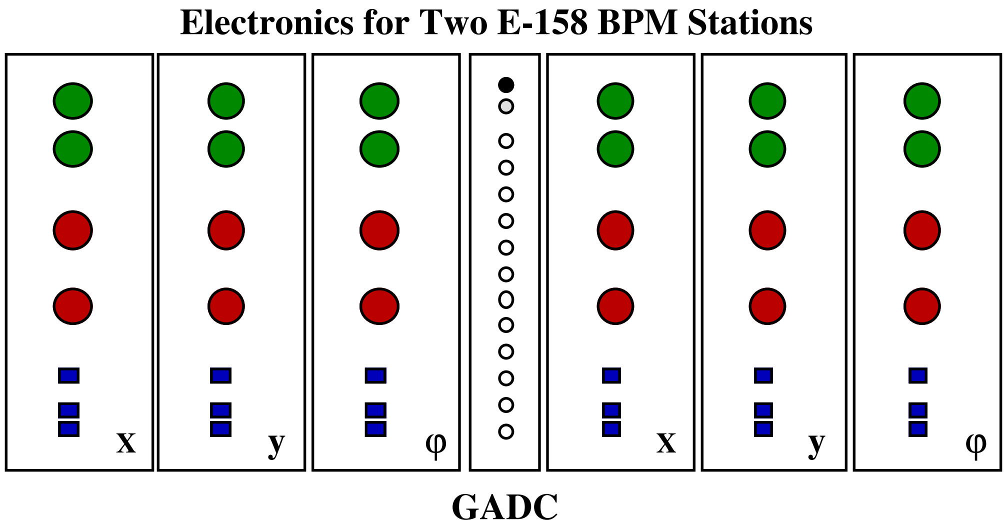

FIGURE 4.4 (b) Lower-budget alternate layout for electronics modules for two BPM Stations employing a commerical 12-channel gated analog-to-digital converter. Spare GADC's would be a must as channels sometimes go bad.

4.3 *Estimate of Components, Equipment & Work Required*

Recording of all signals for 5 BPM stations at 2 bytes per channel amounts to a data rate of 14kB/s and is not an issue. For later analysis, this data should be recorded in a form such that it can easily be correlated with readings from: the toroid(s), luminosity monitor, bunch length monitor. These signals need also to go to the SCP for purposes of buffered data analysis, correlation plot analysis, and history buffering, during commissioning, and for debugging.

Electronics could be probed in between pulses with a calibration signal to check for temperature effects or other drifts. This doubles the required data acquisition rate. If LO's are running CW, the probe signal could simply be triggered in between pulses, and coupled by a 10 dB directional coupler in-line with the cavity signals. In this case the probe amplitude should be 10 dB (+1 dB say) higher than nominal beam signals.For example, during commissioning, the network and the cavities could also be monitored in real time by means of test signals triggered between beam pulses, as indicated in Fig. 2.13.

The following listing does not include general purpose equipment, test & measurement equipment, etc. Here is a list only of the commerical components required for the processor front-end. The Track & Hold units are a separate matter [add]. [Fill in]

Item	QTY	Vendor/Model No.	Unit Cost
Limiter (sma, 1 kW)	10	---	---
Phase-Shifter (sma, knob adjust)	15	---	---
Variable Attenuator (sma, knob adjust)	15	---	---
IQ Mixer (sma)	15	---	---
Isolator (sma)	15	---	---
20 dB coupler (sma)	15	---	---
1/4" Heliax cable	(unknown)	---	---

It should be added that depending on the outcome of a survey of existing, decommissioned cavity BPM electronics modules, it is possible that quite a few of these items could be obtained by scavenging. Most likely the IQ Mixers and limiters could not be obtained in this way.

5. Summary: Tasks to Be Performed

5.1 Recent Studies of A-Line Cavity BPM's - *Draft*

It is useful to summarize here results of cavity BPM studies. A separate note will summarize the disposition of existing cavities, by type and beamline location. For the time being, let us simply note the results, even while some of the unit references may seem a bit crytpic.

Measurements by S. Smith and M. Woods earlier this year showed a combined beam jitter and BPM noise of 15 μm rms. The beam-time request[23] read as follows

Title: Long Pulse High Charge Demonstration
Spokesman: Mike Woods
Purpose of test: Demonstrate $>3\times10^{11}$ electrons in 300 ns pulse to ESA; characterize beam for energy profile, emittance, intensity jitter, position jitter. This is needed for future proposal of Møller scattering experiment.
Description of test apparatus: beam monitors: synchrotron light monitor, toroids, bpms
Beam requirements: 45 GeV, $>3\times10^{11}$ electrons/pulse; 200-400ns pulse width, 10 Hz, $\delta<1\%$.
Space requirements: none
Special power requirements: none
Duration of test: 2 shifts
Desired calendar dates: early May following photocathode reactivation and re-SLEDing of Linac for 30 Hz

Electronics schematic for this experiment corresponds to drawing number $\mathrm{SD}-125-799-00-01$ (draft) for the analog circuitry up to where the signal is sent to ESA for digitization. BPM's inspected prior to the experiment were:

AB01 2420 AB01 2860 AB01 3115 FB31 1010 FB31 1020 FB31 1240

Their intensity scale factors were off by as much as a factor of 3 and AB01 2860 had no data. Best jitter was on FB73 1010 with $\sigma_x = 50\ \mu$m and $\sigma_y = 20\ \mu$m. This is at a location with negligible dispersion and there is also a wire scanner nearby to measure beam size. It was desirable to get a good measurement of beam jitter/beam size there. It is not clear that one should trust the bpm calibration scale given that the intensity scale is off a factor of 3.5 there (bpm read 7.8×10^9 for a real current of 2.3×10^9). It would have been nice to move the beam there a 'known' amount using an upstream corrector to check the scale. And it would be good to look at the signals on a scope.

The relative contributions of processor and other noise were not identified. The beam spot at that location was about 300 μm rms. Wire scanner 50 showed about 300 μm rms spotsize in both x and y. [It should be noted however that wire scanner readings are taken over multiple pulses and thus provide a convolution of jitter and true beam size.] Buffered acquisition data was taken with BPM FB31 1010. For nominal setup and 3.5×10^9/pulse the beam jitter measured 30 μm rms in each of x and y. We then removed 14 dB attenuation from each of x, y, and TMIT. This would reduce the electronics noise contribution by a factor 5. We observed then a reduction by a factor of two, to 15 μm rms. We then removed an additional 6 dB from 'x' only, not 'y' nor

[23] Submitted to and approved by test beam coordinator (Ted Fieguth), chairman, safety oversight committee (Dave Fryberger) area manager (Steve St. Lorant), accelerator dept physicist (Roger Erickson), program coordinator (Clive Field).

'TMIT'. We then measured *x* jitter of 30 μm rms, consistent with 15 μm rms beam jitter. So, we estimate that we have 15 μm rms of beam jitter and 5 μm rms of electronics noise. Hopefully the noise contribution would get proportionately better at high current. For a real beam test, we presumbabely would like to look at 3 BPM cavities in a row and do a fit to them to demonstrate resolution and noise performance.

For future reference, it is not unlikely that we will find that we would like to either (1) replace the MDL-derived phase-signal for this experiment with a phase-cavity derived signal or (2) replace the single-output mixers used (3 per processor) with "IQ" (dual-output) mixers, relegating the role of the MDL derived signal to that of a free-running local oscillator. This is to say that MDL-derived phase errors, cable length drifts, etc. become irrelevant. The rms of the I,Q from each IF port would provide a phase-independent measure of signal amplitude from the cavity port. As is, with the present $SD-125-799-00-01$ (draft) those phase-errors are wrapped into bpm readout errors. Using IQ mixers the only cable lengths that matter are those coming from the three cavities composing one x-y-φ BPM unit. Differential expansion of the three cables from the three cavities to the processor (theoretically zero if the cables are identical in length and subject to the same temperatures) can still cause phase-errors. However, any phase-error contributes only to inference of the sign of the beam offset---said differently it puts a limit on beam position as inferred from a phase versus corrector scan. Generally speaking one would expect a scan of phase versus corrector strength to provide a more accurate monitor of beam-position, particularly in the presence of a "common mode" signal emanating from the cavity. The reason is that it is easier to measure 5° relative to 0, than it is to measure a change in amplitude at the -20 dB level.

5.2 Task to be Performed

As of this draft there remains of a lot legwork to be performed before arriving at a serious taks list for E158 BPM work. A detailed A-Line map is in preparation; it needs to indicate the precise location of existing cavites, by type. Optics analysis, and associated error analysis remain to be performed. A detailed calibration plan for BPM calibration should be developed. In the meantime, it is not settled yet where cavities will be located, nor which will be used. We have merely concentrated on linac-cavities in this note, for the sake of illustration.. If the correct tolerance estimates are somewhere between those estimated here, and those in the proposal, then many questions will evaporate.

Major Questions

Some major questions should be answered first, concerning required BPM resolution. These inform related questions such as:

(1)Should pairing of *x*-cavities be employed to permit symmetrized coupling and common mode subtraction? Can *x*-cavity and *y*-cavity common mode signals be employed to cancel eachother?

(2)Should cavity external Q be increased by means of stub tuners?

(3)Are linac-style cavities really the ones to use?

(4)Is LCW required for temperature stabilization of the cavities? (almost certainly---unless one can be clever in getting tuning errors to cancel at some order).

Let us summarize a list of things to do:

- Finalize estimate of tolerance on angle jitter at target

- Adopt an A-Line configuration for orbit modelling. Subsequent optics analsysis may result in revisions; orbit error analysis will be ongoing.

- Determine parameters for the beam in the linac (would like to have source terms reasonably close to actual parameters to be used). In particular, charge per pulse, and pulse length. Bound jitter in Σ quantities, and confirm that this jitter is negligible

- Finalize a plan for cavities: type, location, and modifications if any. For the time-being, we assume linac-type cavities, symmetrized in pairs.

- Numerical-Circuit Simulation With a Monte Carlo Beam: prepare a sample of 104 or so beams with a good sampling of expected jitter, run them through the cavity model, add in expected temperature drifts, run outputs through an electronics model, and look at scatter versus "true" position. [Include 3dB compression, filter, etc...get real numbers on a scope. Get counts, check bit-noise. Compare model and scope waveform.]

Keeping in mind that we are not ready yet to embark on very time-consuming studies, let us indicate the kind of studies that likely will be in order.

Studies with beam

Studies during SLC running are quite feasible, employing the cavity BPM in Sector 30. Conditions preferred are (1) one beam (2) low charge ($0.5-1\times10^{10}$ electrons per bunch), (3) no BNS (minimal chromatic effects). Conditions of one e^- bunch at LI30 would be required to eliminate cross-talk as a systematic effect, particularly given that the natural cavity discharge time scale (133 ns) is longer than the nominal bunch separation (59 ns). Low-charge simplifies orbit-fitting, diminishing the effect of linac wakefields as a systematic effect. Plan is to compare cavity BPM derived position with the result of linac orbit fitting employing the standard SLC stripline BPM's. Use of the LI25 bunch length monitor will permit correlation study of the form-factor correction. With (1) phase-cavity amplitude and (2) LI25 bunch length monitor (BLM) signal entered in a correlation panel on the SCP, one could take correlation data, with compressor voltage as the step variable in manual acquisition mode.

In addition, use of MDL-derived phase-information could be examined over days by comparison with a φ-cavity signal, and history buffering. The LI30 rack provides the patch panel that sends the MDL signal to the counting house, so study of the MDL signal there is a useful complement to study of the signal from the counting house. The status of this work at present is that the rack and the cable disposition have been visually inspected; the electronics box there is being checked. It is likely that we will simply disconnect the x-y-φ cables from the box, and put in a small bench to work on, with electronics free-standing on the bench. Plenty of spare camac slots are available there; we will locate a GADC for acquisition.

Let us also note that low-charge, "test-beam" running in the A-Line is most likely not a useful condition for cavity studies (unless still other electronics are to be employed for those tests). At least 100 pC of charge in one fill time is probably a minimal requirement.

Studies on the "bench"

One could contemplate removal and bench measurement on each cavity. This is a lot of work, and could actually compromise the cavities. We put aside for now this question. One could perform studies of the various cable networks, without beam, as in Fig. 2.13, for example.

At some much higher level of refinement, one is interested to deal with matters such as: (1)assess aperture and operability (2)setup a work bench area in the counting house (3) revisions to front-end electronics (10MHz IF?) (4) assemble documentation, digital camera photos and graphics, ESA BPMs, with a user manual. Far beyond that one may imagine much to do: (1)Assess jitter and sources of jitter by means of great cleverness (dither injector parameters at 1 Hz, employ a lock-in amplifier on-mixed down pickup?) (2) Calibrate all A-Line correctors, employing bend calibrations, traceable to spin-rotation calibration (3)Survey cavities in-situ, assess Cavity rotation and tilt. (4) Without beam, probe the MDL from the counting house, using an off-frequency CW sine-wave and a lock-in amplifier to monitor the reflected amplitude and phase from the vicinity of LI00.

Equipment & Personnel

Since we are at a very preliminary stage, it is hard to provide a rigorous accounting for the total effort. Let us make a guess-timate. We suppose that cavity temperature regulation at the level of 1° F is required, so that LCW (linac cooling water) hookups must be provided, where not already present. Tube routings appear to thread each 3-cavity set; some tests from upstairs could check the efficacy of this temperature stabilization. We suppose that cavity tune should be monitored via network analysis from upstairs, as an input to error tracking. We suppose that over 30 years, the cavities have not been so mistuned by rough handling, work hardening, or other effects that they cannot be tuned correctly via LCW.

With these assumptions we make a list. Items marked by "$" correspond to commerical component or instrument purchases. Items marked by "↵" are available on-site if their owners can be convinced to part with them temporarily (if not, "↵" should be replaced with "$"). Items marked by "⇐" aren't off the shelf items and require significant work. Mechanical, electrical or other engineering work is marked by "FTE", implying some fraction of an FTE.

Facilities-Related

LCW	FTE
cabling (may not be required, pending inspection)	FTE
cavity relocation, install, rough align, hookups, vacuum, align	FTE

Temporary Equipment for the Rack Area, During Commissioning and Testing

S-Band Network Analyzer	↵
Spectrum Analyzer (3 GHz or higher)	↵
MAC w/Labview	↵
Prototype BPM Processors	⇐ $, FTE

Permanent Equipment for the Rack Area, During Commissioning, Testing, Running

Five BPM Processor Units (to be designed)	⇐ $, FTE
4-Channel Scope, 400 MHz or higher	↵
Frequency Synthesizing Signal Generator (10 MHz - 3 GHz or higher)	↵
S-Band Microwave Kit: spare mixers, limiters, phase-shifters, isolators	$
scope camera	$

Software & Electronics

At some point the question may arise of a VXI crate, modules and time for VTEST software development. No opinion on this yet; it has proved helpful in other work of this sort though.[more work needed on description of Ni T&H]